Molecular Therapy
Original Article

dCas9-Based *Scn1a* Gene Activation Restores Inhibitory Interneuron Excitability and Attenuates Seizures in Dravet Syndrome Mice

Gaia Colasante,[1,7] Gabriele Lignani,[2,7] Simone Brusco,[1] Claudia Di Berardino,[1] Jenna Carpenter,[2] Serena Giannelli,[1] Nicholas Valassina,[1] Simone Bido,[1] Raffaele Ricci,[1] Valerio Castoldi,[3] Silvia Marenna,[3] Timothy Church,[2] Luca Massimino,[1] Giuseppe Morabito,[1] Fabio Benfenati,[4,5] Stephanie Schorge,[2] Letizia Leocani,[3] Dimitri M. Kullmann,[2] and Vania Broccoli[1,6]

[1]Stem Cell and Neurogenesis Unit, Division of Neuroscience, San Raffaele Scientific Institute, 20132 Milan, Italy; [2]Department of Clinical and Experimental Epilepsy, UCL Institute of Neurology, University College London, Queen Square, London WC1N 3BG, UK; [3]Experimental Neurophysiology Unit, Institute of Experimental Neurology (INSPE), San Raffaele Scientific Institute, 20132 Milan, Italy; [4]Center for Synaptic Neuroscience and Technology, Istituto Italiano di Tecnologia, 16132 Genova, Italy; [5]IRCCS Ospedale Policlinico San Martino, University of Genova, 16132 Genova, Italy; [6]CNR Institute of Neuroscience, 20129 Milan, Italy

Dravet syndrome (DS) is a severe epileptic encephalopathy caused mainly by heterozygous loss-of-function mutations of the *SCN1A* gene, indicating haploinsufficiency as the pathogenic mechanism. Here we tested whether catalytically dead Cas9 (dCas9)-mediated *Scn1a* gene activation can rescue *Scn1a* haploinsufficiency in a mouse DS model and restore physiological levels of its gene product, the $Na_v1.1$ voltage-gated sodium channel. We screened single guide RNAs (sgRNAs) for their ability to stimulate *Scn1a* transcription in association with the dCas9 activation system. We identified a specific sgRNA that increases *Scn1a* gene expression levels in cell lines and primary neurons with high specificity. $Na_v1.1$ protein levels were augmented, as was the ability of wild-type immature GABAergic interneurons to fire action potentials. A similar enhancement of *Scn1a* transcription was achieved in mature DS interneurons, rescuing their ability to fire. To test the therapeutic potential of this approach, we delivered the *Scn1a*-dCas9 activation system to DS pups using adeno-associated viruses. Parvalbumin interneurons recovered their firing ability, and febrile seizures were significantly attenuated. Our results pave the way for exploiting dCas9-based gene activation as an effective and targeted approach to DS and other disorders resulting from altered gene dosage.

INTRODUCTION

Dravet syndrome (DS) is a severe epileptic encephalopathy beginning in the first year of life with seizures often associated with fever that evolve into frequent, prolonged, and clustered epileptic crises.[1–3] In subsequent years, patients often develop psychomotor delay, behavioral disturbances, and cognitive impairment.[4] DS is a genetic condition mainly caused by mutations in the *SCN1A* gene encoding for the $Na_v1.1$ voltage-gated sodium channel α subunit.[5,6] Over 650 missense and nonsense *SCN1A* mutations have been described in DS patients. Although most are *de novo*, some mutations have been found to be inherited in familial cases.[7] *SCN1A* mutations affect only one copy of the gene, typically leading to loss of function and indicating that a haploinsufficient genetic mechanism is responsible for DS. These data suggest that a reduced amount of $Na_v1.1$ channel impairs neuronal activity and function. *Scn1a* heterozygous mutant mice display similar neurological symptoms, including severe epilepsy, behavioral alterations, and premature death.[8–11] Functional studies revealed that cortical fast-spiking GABAergic inhibitory interneurons exhibit reduced intrinsic excitability and defects in action potential firing.[8,10,12] In contrast, both excitability and firing of cortical excitatory neurons from *Scn1a* heterozygous mutant mice appear to be substantially unaltered.[8,13] These findings potentially resolve the paradox that epilepsy arises from loss-of-function mutations in $Na_v1.1$, which contributes to the fast depolarization of neuronal membranes during an action potential. Of note, $Na_v1.1$ has been found to be mainly expressed in inhibitory interneurons by immunohistochemistry analysis, suggesting that this sodium channel isoform has a preponderant function in that neuronal population.[10] Accordingly, selective inactivation of *Scn1a* in cortical interneurons is sufficient to elicit neurological deficits comparable with those described in constitutive mutant mice,[14,15] and, conversely, *Scn1a* loss restricted to the dorsal-telencephalic (e.g., neocortical, hippocampal) excitatory neurons has ameliorating effects on epileptic seizures and sudden death.[13] *Scn1a* heterozygous mutant mice develop spontaneous and recurrent seizures starting from 3 weeks after birth, often leading to

Received 19 April 2019; accepted 27 August 2019;
https://doi.org/10.1016/j.ymthe.2019.08.018.

[7]These authors contributed equally to this work.

Correspondence: Vania Broccoli, Stem Cell and Neurogenesis Unit, Division of Neuroscience, San Raffaele Scientific Institute, Via Olgettina 58, 20132 Milan, Italy.
E-mail: broccoli.vania@hsr.it
Correspondence: Gaia Colasante, Stem Cell and Neurogenesis Unit, Division of Neuroscience, San Raffaele Scientific Institute, Via Olgettina 58, 20132 Milan, Italy.
E-mail: colasante.gaia@hsr.it

premature and sudden death.[8–10] Remarkably, body temperature elevation triggers myoclonic and generalized seizures in these mice, recapitulating febrile seizures in DS patients.[16] Thus, DS mice represent a valuable model of the disease, not only to dissect the pathological mechanisms but also to evaluate the efficacy of innovative therapies. Drug treatment of DS patients, including stiripentol in combination with clobazam and valproate, has limited efficacy and poorly controls convulsive seizures.[17,18] Cannabidiol or serotonin uptake inhibitors have been reported to reduce seizure frequency in some patients, but larger studies are needed to appreciate the exact therapeutic indications for these treatments.[19–21] Nonetheless, complete seizure cessation is rarely obtained with any of these pharmacological anticonvulsants. Gene therapy approaches for neurodevelopmental disorders are in rapid development because of the introduction of novel serotypes of recombinant adeno-associated viruses (AAVs), allowing efficient transduction of neurons.[22] However, the *SCN1A* coding sequence is 6 kb long, exceeding the strict cargo limit for AAVs. Although lentiviruses (LVs) can carry the *SCN1A* gene sequence, they show limited spread in neural tissue and are therefore inadequate to treat diseases affecting large brain areas.[23] These obstacles have prevented substantial advances in gene-based therapies for DS. Given that one copy of the *SCN1A* gene is still functional in DS, stimulating its endogenous expression over physiological levels might lead to increased availability of the $Na_v1.1$ channel protein, potentially leading to symptomatic improvement. Thus, a system able to induce *SCN1A* gene expression in neurons in a regulated manner, without significant off-target effects, would be a strong therapeutic candidate tool for DS.

CRISPR-Cas9 technology has become a powerful tool for genome editing, allowing DNA to be targeted with high efficiency and specificity. As demonstrated by pioneering works in several cell types and organisms, the Cas9/single guide RNA (sgRNA) complex can efficiently generate double-strand breaks, which then trigger non-homologous end joining-mediated gene knockout or homology-directed repair-mediated recombination.[24–26] A modified version of the CRISPR-Cas9 system has been developed by generating a nuclease-dead Cas9 (dCas9) fused to effector domains for transcriptional gene regulation. Hence, the dCas9/sgRNA complex has provided a crucial platform for programming diverse types of transcriptional or epigenetic manipulation of the genome without cleaving the target DNA.[27–29] Seminal studies have shown that dCas9-based gene activation is highly specific in DNA binding and gene regulation and promotes chromatin remodeling of the regulatory elements of the gene of interest.[30–32] This system has been successfully implemented to investigate hierarchies in gene regulatory networks, screening for cellular phenotypes and directing somatic cell fate.[33–36] In the activatory CRISPR system, dCas9 is fused to multiple VP16 transcriptional activator domains that robustly boost gene transcription when combined with one or more sgRNAs targeting sequences in the proximal promoters or close to transcription start sites (TSSs).[26,36,37] As proof of concept, this technology has also been employed to activate endogenous genes in mouse models of disease to ameliorate biomarkers of diabetes, muscular dystrophy, and acute kidney disease.[30] More recently, it has been applied to enhance expression of the *Sim1* gene in the hypothalamus and to rescue the associated obesity phenotype.[38] Here we describe a dCas9-based system that significantly upregulates *Scn1a* expression and restores $Na_v1.1$ protein levels in both cellular and animal models of DS. This targeted gene activation rescues membrane excitability and action potential firing in DS cortical interneurons and significantly attenuates hyperthermia-induced seizures in DS mice.

RESULTS

A Single sgRNA Enhances *Scn1a* Gene Expression by Targeting Its Proximal Promoter

To achieve upregulation of *Scn1a* gene transcription, we sought to define the necessary dCas9/sgRNA elements by a candidate approach *in vitro*. Through an extensive bioinformatics analysis, we determined the *Scn1a* gene promoter regions to focus the sgRNA design. Several studies have pointed out that sgRNAs can transactivate genes of interest more efficiently when localized within 500 bp from the gene TSS.[34] We interrogated the Encyclopedia of DNA Elements (ENCODE) and Fantom5 databases for the expression profiling and epigenetic marks of actively transcribed genes in the adult mouse brain. In addition, CAGE-seq and DNase-seq datasets were queried to determine the exact TSSs for *Scn1a* (Figure S1). We identified two regions in the *Scn1a* locus where RNA polymerase II (Pol II), mono- and trimethylation of lys4, and acetylation of lys27 of H3 histone were strongly enriched and revealed DNase I-hypersensitive sites. CAGE-seq peaks were aligned to the same sequences, confirming the existence of two active TSSs (TSS1 and TSS2) located upstream of two non-coding exons (exon A and exon B) (Figure S1) and producing two different mRNA isoforms, both expressed in the adult mouse brain.[39] 200 bp upstream of the exon A (distal promoter) and 250 bp upstream of exon B (proximal promoter) (Figure 1A) were submitted to the CRISPOR web tool (http://crispor.tefor.net) for sgRNA design. We selected five guides in the distal promoter and six in the proximal one with specificity scores higher than 50% (Figures 1B and 1C; Table S1). Then we determined whether dCas9 fused to VP160 (dCas9-VP160), a transcriptional activator that carries 10 tandem copies of VP16 (a herpes simplex virus type 1 transcription factor), in association with the selected sgRNAs was able to upregulate *Scn1a* gene expression in the P19 murine teratocarcinoma cell line. sgRNAs specific for *Scn1a* promoters and one control guide (sgCtrl), targeting the β-galactosidase bacterial sequence, were cloned into the pU6 vector and individually lipofected into P19 cells together with the Ef1a-dCas9-VP160-T2A-GFP (Figure 1D), and 3 days later, after ascertaining GFP expression, cells were harvested for RNA extraction and qRT-PCR (Figure 1D). Interestingly, none of the sgRNAs targeting the distal promoter were able to significantly alter the basal expression of *Scn1a* (Figure 1E). Conversely, among the guides targeting the proximal promoter, only sg1P was found to significantly increase *Scn1a* mRNA levels with respect to sgCtrl (Figure 1F). Comparable results were obtained when sgRNAs were lipofected with dCas9 linked to a puromycin resistance cassette

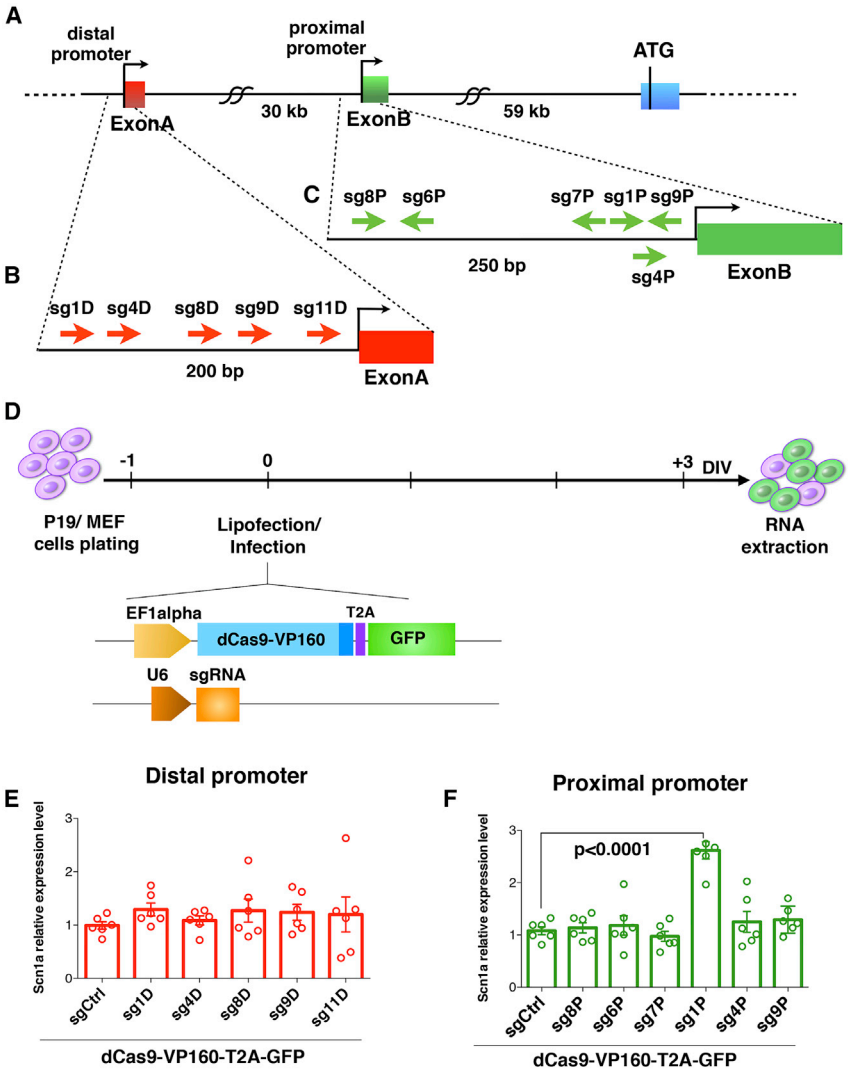

Figure 1. sgRNA Design and Screening for Stimulating *Scn1a* Gene Expression with the dCas9 Activation System in P19 Cells

(A–C) Schematic representation of the *Scn1a* gene (A) with distal (B) and proximal (C) promoter regions; the positions of the sgRNAs selected for this screening are highlighted. (D) Experimental setting for the sgRNA screening in P19 cells and schematic representation of the constructs employed for cell lipofection. One day after plating, P19 cells were lipofected, and the subsequent day, GFP expression was ascertained. At 3 DIV, the cells were processed for RNA extraction. (E and F) qRT-PCRs for *Scn1a* mRNA levels performed on RNA extracted from P19 cells lipofected with dCas9VP160-T2A-GFP together with sgRNAs targeting the distal (E) or proximal (F) promoter. Data are normalized on the 18S rRNA and relative to sgCtrl-lipofected cells. sg1p induces significant upregulation of *Scn1a* compared with sgCtrl ($n = 6$, $p < 0.0001$, one-way ANOVA followed by Bonferroni multiple comparisons test). Data are shown as mean ± SEM, with dots representing individual samples.

(Ef1a-dCas9-VP160-T2A-Puro^R) and puromycin was added to the culture medium the day after transfection (Figures S2A–S2C), indicating that antibiotic selection and consequent enrichment of lipofected cells were not strictly necessary to detect sg1P-mediated *Scn1a* induction. sg1P upregulated *Scn1a* gene expression to a similar extent in primary mouse embryonic fibroblasts (MEFs) (Figure S2D). In conclusion, we identified sg1P as an sgRNA that is sufficient, when associated with the dCas9 activation system, to stimulate basal transcription of *Scn1a* consistently in different cell types.

sg1P/dCas9-VP160 Lentiviral Transduction Upregulates *Scn1a* Expression in Primary Neurons

We asked whether the sg1P/dCas9-VP160 system could stimulate *Scn1a* expression in primary hippocampal neurons. Neurons were co-transduced with Ef1a-dCas9VP160-T2A-GFP and pU6-sg1P or pU6-sgCtrl LVs the day after plating to maximize transduction efficiency (Figure 2A). Immunofluorescence analysis performed at 10 days *in vitro* (DIV) showed that almost 50% of the plated neurons were transduced (Figure 2B). With this intermediate efficiency, we decided to purify the infected cells to obtain reliable information regarding the regulation of *Scn1a* expression. Thus, 10 DIV transduced GFP$^+$ neurons from sgCtrl- and sg1P-treated samples were isolated by fluorescence-activated cell sorting (FACS) (Figure 2C), and the RNA was extracted for gene expression analysis. *Scn1a* expression levels were robustly increased when transduced with sg1P with respect to sgCtrl (Figure 2D). However, FACS is detrimental to neurons and prevents their functional analysis. For this reason, we generated a single lentiviral vector carrying both sg1P and dCas9-VP160 (Figure 2E), which improved transduction efficiency up to ~75% (Figure 2F). In this setting, a 4-fold increase in *Scn1a* expression was detected in sg1P with respect to sgCtrl-treated neurons. Moreover, no alteration in the transcriptional levels of the second *Scn1a* mRNA isoform carrying exon A was detectable (Figure 2G), indicating that the sg1P/dCas9-VP160 activation system does not affect the transcriptional status of the distal promoter. To evaluate whether increased transcription of *Scn1a* led to higher $Na_v1.1$ protein levels, we performed western blot analysis of membrane lysates isolated from transduced 10 DIV primary neuronal cultures, which showed a 2-fold increase in membrane-associated $Na_v1.1$ protein (Figure 2H).

Taken together, these results indicate that sg1P associated with the dCas9 activation system can modulate *Scn1a* gene activity in primary neurons and, accordingly, increase the levels of the $Na_v1.1$ channel protein.

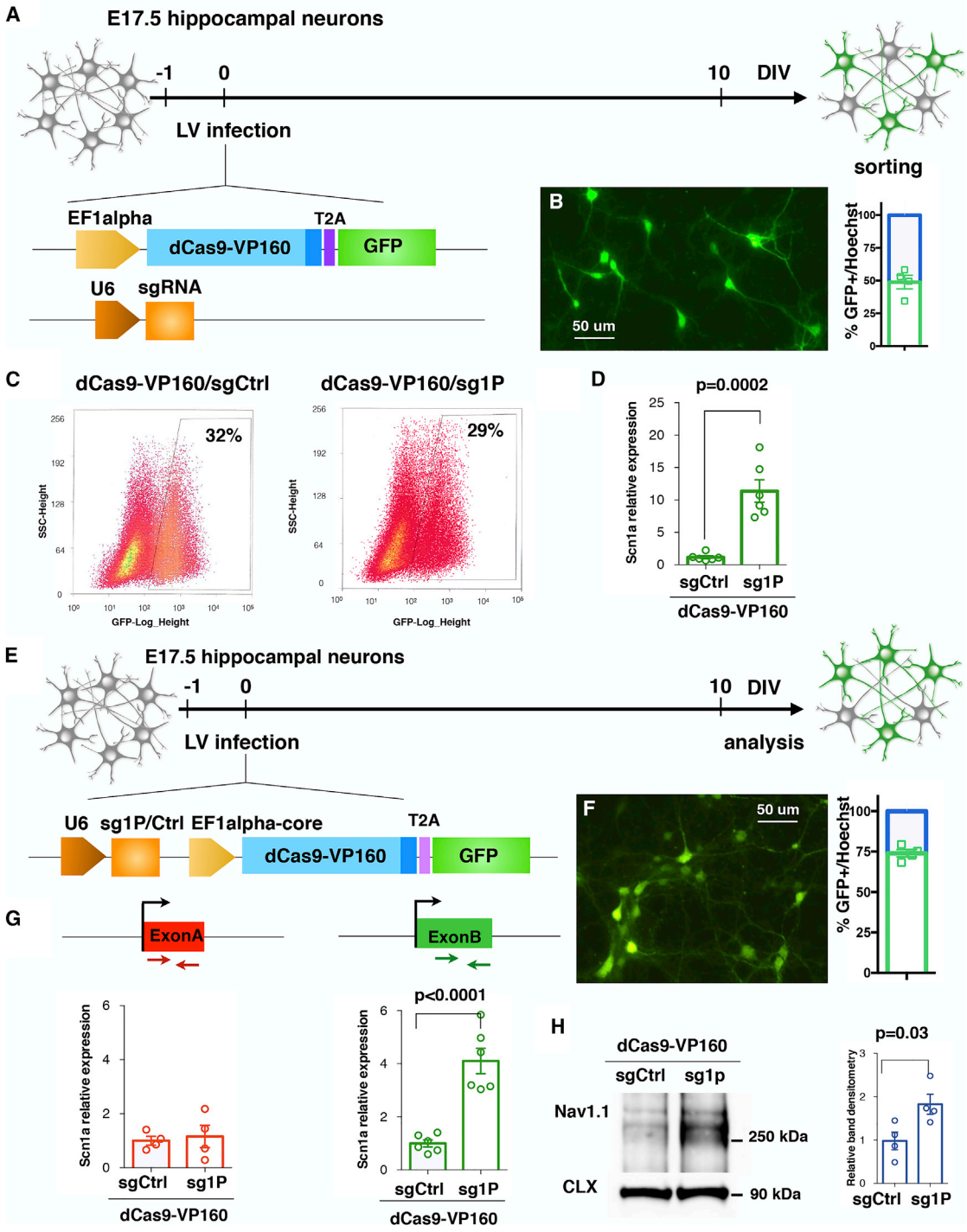

Figure 2. dCas9-VP160/sg1P Potentiates *Scn1a* Gene Transcription in Primary Hippocampal Neurons

(A) Schematic drawing depicting the experimental setting to deliver the Ctrl- and *Scn1a*-dCas9A system in primary neurons. Hippocampal neurons were derived from E17.5 embryos and, the day after plating, were co-transduced with two distinct lentiviruses (LVs) carrying Ef1a-dCas9-VP160- T2A-GFP and pU6-sg1P or pU6-sgCtrl guides, respectively. (B) Representative image of anti-GFP immunofluorescence at 10 DIV and quantification of GFP^+ transduced neurons over the total cell number. Scale bar, 50 μm. (C) Representative FACS images of GFP^+ neurons transduced with either the sgCtrl- or sg1P-dCas9 activation system. (D) qRT-PCR reveals the increased *Scn1a* transcriptional levels in hippocampal neurons infected with sg1P with respect to sgCtrl conditions (n = 6, p = 0.0002, Student's t test). Data are shown as mean ± SEM, with dots representing individual samples. (E) Schematic setting of E17.5 neurons transduced with a LV carrying both the pU6-sgRNA cassette and dCas9-VP160-T2A-GFP

(legend continued on next page)

dCas9-Based Gene Activation Is Highly Specific for *Scn1a* in Primary Neurons

We examined the specificity of the dCas9 activation system by assessing global gene expression in primary neurons transduced with dCas9-VP160 together with either sg1P or sgCtrl. RNA sequencing (RNA-seq) was performed on 3 DIV neurons 2 days after lentiviral transduction with either sg1P or the sgCtrl (Figure 3A). Notably, the only gene with significantly increased expression relative to the control was *Scn1a* (log2 fold change > 1.5, $p < 0.005$), indicating the high specificity of the dCas9 activation system in primary neuronal cells (Figures 3B, red dots). CRISPOR provided a list of 195 putative off-target genes associated with sg1P. Because dCas9A is nuclease defective, we reasoned that aspecific transcription activation could occur only when off-target sequences were in close proximity to TSSs of genes. Therefore, we filtered the list using the web tool Galaxy to investigate which of those putative off-targets were located within 500 bp of TSSs of any annotated gene. Only 4 of 195 putative off-target genes were identified in the putative promoter regions upstream of the *Prp4*, *BC02*, *Olfr919*, and *Plrg1* genes. However, as shown by both sequencing and qRT-PCR analyses, the expression of these genes was not altered after delivery of the dCas9 activation system (Figures 3B and 3C, left panel, yellow dots).

Absolute and relative levels of the various Na_v α subunits are strictly regulated, allowing a fine balance of neuronal membrane excitability.[40] Therefore, we examined the expression of other Na_v α subunit-encoding genes. The global transcriptional analysis revealed no significant changes in their expression levels (Figure 3B, right panel, yellow dots). These results were confirmed by qRT-PCR assays of independent cellular replicates (Figure 3C, right panel). In conclusion, the global and targeted gene expression analyses of primary neurons transduced with the sg1P-dCas9 activation system (hereafter called *Scn1a*-dCas9A) confirmed the high specificity for *Scn1a* gene transactivation at a genome-wide level.

dCas9-Based *Scn1a* Gene Activation Enhances Neuronal Activity in Immature Wild-Type (WT) Cortical Interneurons

To evaluate whether the increased levels of $Na_v1.1$ protein in primary neurons were sufficient to alter neuronal excitability, whole-cell patch-clamp experiments were carried out in dCas9A-transduced neurons. We conceived a dual LV-inducible system designed with a first lentivector carrying dCas9-VP160 with the tdTomato reporter regulated by the reverse tetracycline-controlled transactivator (rtTA)-responsive element (TRE) and a second lentivector carrying the transactivator rtTA and sgRNAs (sg1P or sgCtrl) to explore a setting that would be relevant in *in vivo* experiments (Figure 4A; Figure S3A). Indeed, the split of *Scn1a*-dCas9A in two vectors is required for *in vivo* delivery mediated by AAVs, characterized by a limited cargo capacity. In this setting, upon doxycycline (dox) administration, about 60% of neurons were transduced (Figure S3B). A 2-fold increase in the basal level of *Scn1a* gene expression (*Scn1a*-dCas9A versus Ctrl-dCas9A) in WT neurons at 7 DIV was observed upon dox administration (Figure S3C, +dox), but not under dox-absent conditions (−dox), although some leaky expression of dCas9A could be detected (Figure S3D).

Because $Na_v1.1$ channel loss mainly affects GABAergic interneurons, we established primary neuronal cultures from GAD67-GFP mouse embryos that were transduced with either the Ctrl-dCas9A or *Scn1a*-dCas9A system and analyzed when double-positive for GFP and tdTomato (Figures 4A and 4B).

First recordings were performed on 9–11 DIV primary neurons before their achievement of full functional maturation. Current step injections showed a significant increase in firing rate in interneurons transduced with the *Scn1a*- compared with the Ctrl-dCas9 activation system (Ctrl-dCas9A, n = 11; *Scn1a*-dCas9A, n = 15; $p = 0.03$, Mann-Whitney non-parametric t test) (Figures 4C–4E; Figure S4). No alteration of neuronal firing rate was mediated by *Scn1a*-dCas9A in the absence of dox (Figure S3E). These results underline the potential efficiency of *Scn1a*-dCas9A to increase interneuron excitability upon alteration of *Scn1a* gene dosage, at least in an immature network.

Recently, we developed a new electrophysiological approach ("activity clamp") to analyze how a neuron in a given epileptic network responds to antiepileptic drugs.[41] Here we modified this method to adapt it for primary neuronal cultures to compare interneurons transduced with either the Ctrl-dCas9A or *Scn1a*-dCas9A system. First, we recorded in interneurons the barrage of α-amino-3-hydroxy-5-methyl-4-isoxazolepropionic acid (AMPA) receptor-mediated excitatory synaptic currents that occurs in the presence of the chemoconvulsant potassium channel blocker 4-aminopyridine (4-AP). Then we converted the recorded currents into a conductance waveform, and, by applying dynamic current clamp, we fed them back to interneurons pharmacologically isolated from the network. We then compared neurons transduced with either the *Scn1a*- or Ctrl-dCas9A system (Figures 4F–4I). Activity clamp showed that GABAergic interneurons transduced with *Scn1a*-dCas9A exhibited an increase in the number of action potentials (APs) evoked by the same epileptic inputs as well as higher firing frequencies reached during the protocol (Ctrl-dCas9A, n = 10; *Scn1a*-dCas9A, n = 12; $p = 0.0009$, parametric Student's t test) (Figure 4I). Altogether, these results indicate that increased expression of *Scn1a* obtained by the dCas9A system is

sequence under control of the EF1alpha core promoter. (F) Anti-GFP immunofluorescence at 10 DIV and relative quantification of transduced GFP^+ cells over total, showing that a single LV reaches a transduction efficiency of 75%. Scale bar, 50 μm. (G) qRT-PCR for *Scn1a* with primers amplifying the first (exon A) and second 5′ UTR exon (exon B). Data are normalized on 18S rRNA and expressed as relative to sgCtrl. Exon A, sg1P versus sgCtrl: $p = 0.7353$; exon B, sg1P versus sgCtrl: $p < 0.0001$; Student's t test). (H) Left: western blot for $Na_v1.1$ and Calnexin on protein lysates from Ctrl-dCas9A- and *Scn1a*-dCas9A-treated neurons at 10 DIV. Right: quantification obtained through densitometry and normalized on Calnexin levels and expressed as *Scn1a*-dCas9A relative to Ctrl-dCas9A (data are shown as mean ± SEM, with dots representing individual samples); n = 4; sg1P versus sgCtrl: $p = 0.03$, Student's t test.

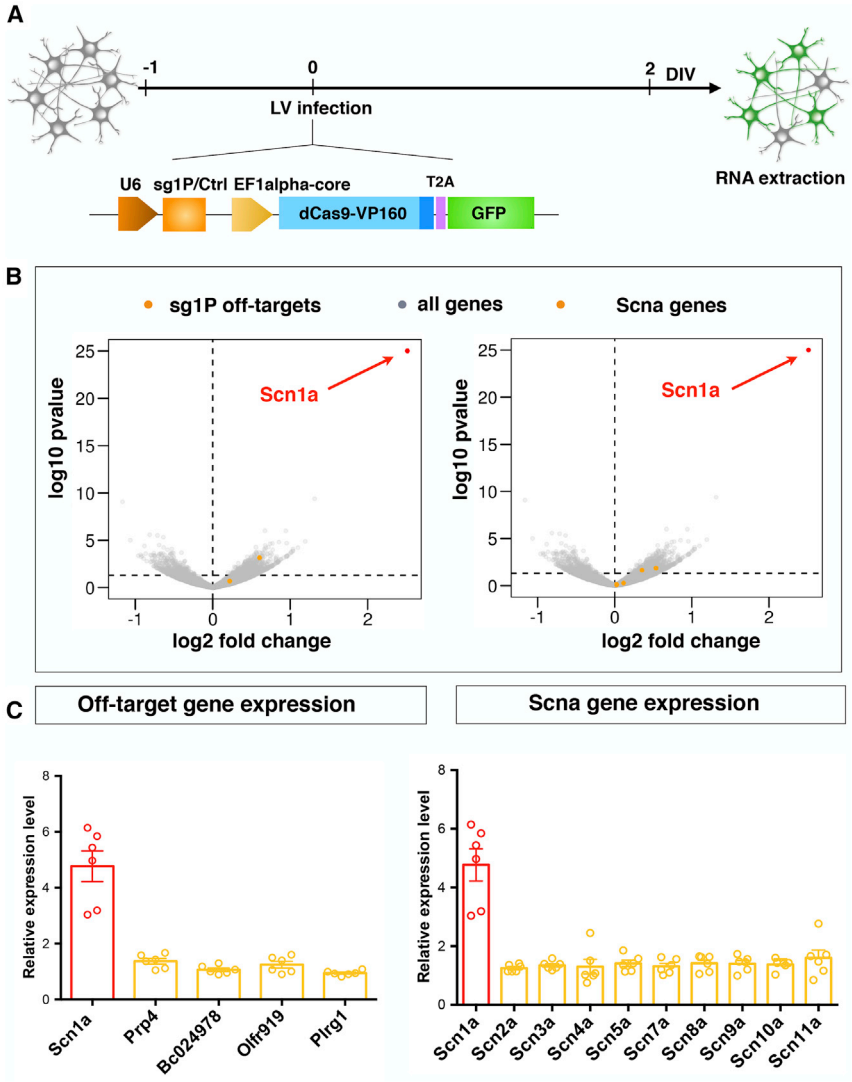

Figure 3. Global Gene Expression analysis of Transduced Neurons Confirms the High Specificity Profile of the *Scn1a*-dCas9A System

(A) Schematic view of the experimental setting to perform gene expression profiling of Ctrl-dCas9A- and *Scn1a*-dCas9A-treated primary neurons. E17.5 embryo-derived neurons were transduced with single LVs at DIV 1 expressing either the Ctrl-dCas9A or *Scn1a*-dCas9A elements and processed for RNA extraction 48 h later (DIV 3). (B) Volcano plots showing the log10 p value as a function of log2 fold changes in gene expression in *Scn1a*-dCas9A-treated neurons with respect to Ctrl-dCas9A. *Scn1a* is shown as a red dot. Yellow dots represent off-target genes in the left panel and other *Scna* genes in the right panel. All other genes are shown as gray dots. (C) qRT-PCRs for profiling the expression of predicted off-targets (genes *Prp4, BC024978, Olfr919*, and *Plrg1*; left panel) or other *Scna* genes (*Scn2a, Scn3a, Scn4a, Scn5a, Scn7a, Scn8a, Scn9a, and Scn11a*; right panel). Plotted values are normalized on 18S rRNA and expressed as relative to sgCtrl-treated samples (value = 1, data not shown). n = 6; sg1p versus sgCtrl $p < 0.0004$, Student's t test. Data are shown as mean ± SEM, with dots representing individual samples.

sufficient to increase interneuron excitability in response to epileptiform barrages of synaptic excitation.

dCas9-Based *Scn1a* Activation Increases $Na_v1.1$ Protein Levels and Rescues Excitability in *Scn1a*$^{+/-}$ Mutant Cortical Interneurons

The experiments described above show that the *Scn1a*-dCas9A system upregulates *Scn1a* expression in WT interneurons, increasing $Na_v1.1$ protein levels and enhancing their excitability. We asked whether this system could also boost transcription of the single WT *Scn1a* allele in DS mice to reach sufficient $Na_v1.1$ protein levels to compensate for haploinsufficiency and attenuate the pathology.

We tested the efficacy of the *Scn1a*-dCas9A system in *Scn1a*$^{+/-}$ neurons derived from a DS mouse model (Figure 5A).[10] Considering that the *Scn1a* gene starts to be expressed around post-natal day 10 (P10),[10,42] the analysis was done at DIV 22–25 to ensure display of the characteristic DS phenotype. Interestingly, at this time point, WT neurons seemed to be unresponsive to *Scn1a*-dCas9A treatment (Figure 5B), whereas we observed a 3.5-fold increase in levels of *Scn1a* expression in *Scn1a*-dCas9A- compared with Ctrl-dCas9A-treated DS neurons (Figure 5C). To assess the nature of *Scn1a*-dCas9A-induced mRNA, we performed deep sequencing of PCR amplicons spanning the mutation region and found out that, in Ctrl-dCas9A-transduced neurons corresponding to basal conditions, WT and mutant transcripts were approximately equally abundant (almost 50% each) (Figure 5D). The same relative proportion was maintained in *Scn1a*-dCas9A-treated neurons (Figure 5D). These data indicate that mutant mRNA is stable in DS neurons and, consequently, that *Scn1a*-dCas9A treatment induces upregulation of both transcripts. However, at the protein level, untreated *Scn1a*$^{+/-}$ postnatal brains showed an ~50% reduction in $Na_v1.1$ protein levels with respect to the control counterparts (Figures 5E and 5F). In accordance with mRNA data, the levels of $Na_v1.1$ protein did not change upon *Scn1a*-dCas9A treatment in *Scn1a*$^{+/+}$ neurons, whereas, remarkably, *Scn1a*-dCas9A-treated *Scn1a*$^{+/-}$ neurons exhibited almost doubled $Na_v1.1$ protein levels compared with Ctrl-dCas9A-treated *Scn1a*$^{+/-}$ neurons at 25 DIV (Figures 5E and 5F). An immunoblot signal lower than 170 kDa and corresponding to truncated $Na_v1.1$ protein was not observed, neither in *Scn1a*$^{+/-}$ adult brains nor in *Scn1a*$^{+/-}$ neurons under basal conditions (Ctrl-dCas9A) or treated with Scn1a-dCas9A (Figure 5E). These results imply that the mutant protein is likely

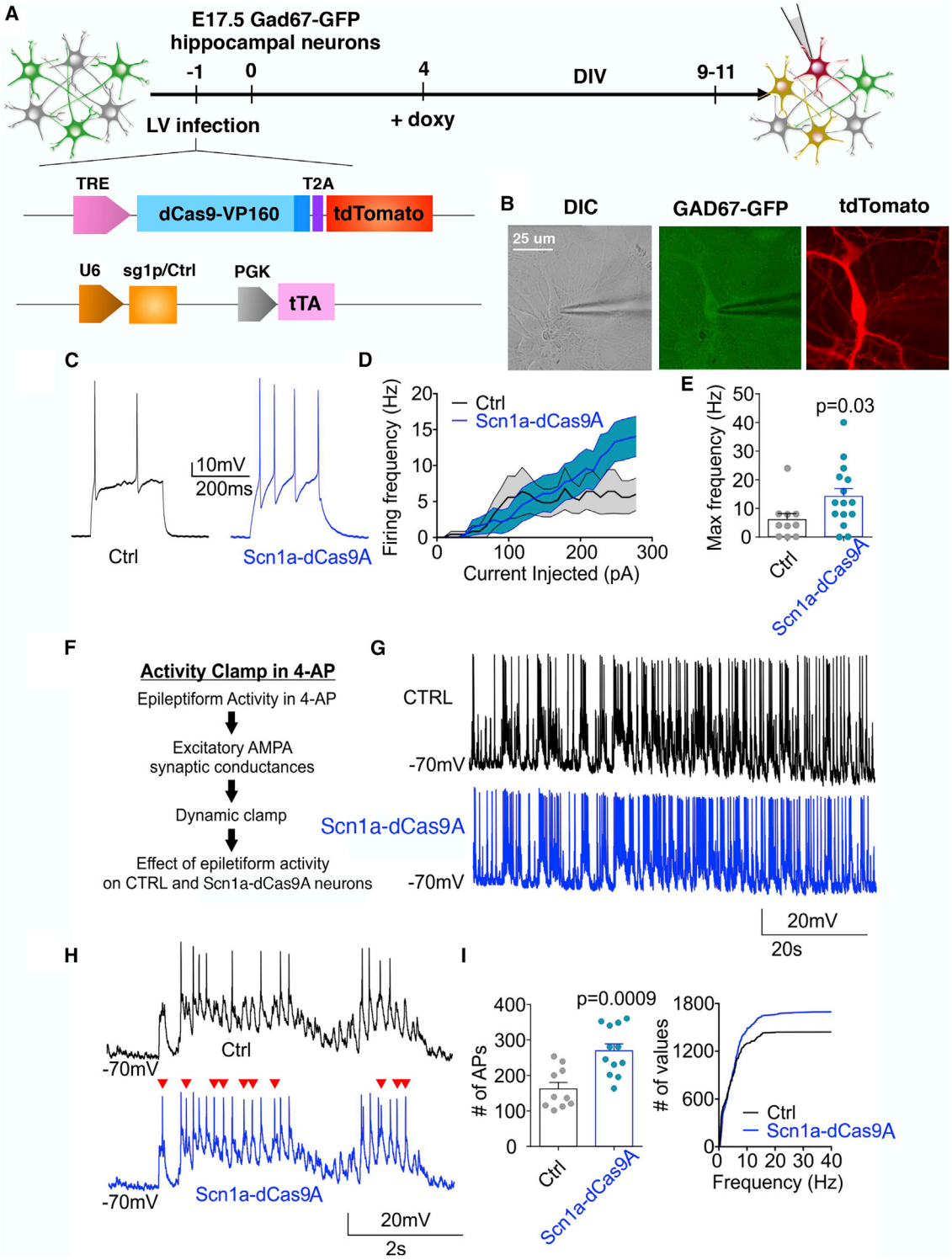

Figure 4. *Scn1a*-dCas9A Increases Neuronal Excitability in Cortical Immature Wild-Type Interneurons

(A) Schematic drawing showing the timeline of transduction with LVs expressing the dCas9A systems on primary wild-type GAD67-GFP neurons and their subsequent functional analysis. (B) Representative images of a patch-clamp-recorded interneuron expressing both GFP under the GAD67 promoter and tdTomato, reflecting the active *Scn1a*-dCas9A system. Scale bar, 25 μm. (C) Representative current-clamp traces of APs induced by a single current step in dCas9A (black trace, sgCtrl) or *Scn1a*-dCas9A interneurons (blue trace, sg1P). (D) Firing frequency versus injected current for Ctrl- and *Scn1a*-dCas9A-transduced interneurons (Ctrl-dCas9A, n = 11; *Scn1a*-dCas9A,

(legend continued on next page)

degraded and not targeted to the plasma membrane. To assess whether rescue of $Na_v1.1$ protein levels has a functional effect on DS neurons, electrophysiological experiments were repeated in *Scn1a*$^{+/-}$;GAD67-GFP GABAergic interneurons transduced either with the Ctrl-dCas9A or *Scn1a*-dCas9A system (Figures 6A and 6B). Recordings were performed on 18–20 DIV neuronal cultures to treat fully mature and functional interneurons. Current step injections showed a decreased frequency-current relationship and maximum AP frequency in *Scn1a*$^{+/-}$ interneurons compared with the WT when both were transduced with the Ctrl-dCas9A system (Figures 6C–6E). Accordingly, an increased current threshold to trigger a single AP was observed (Figure 6G). These defects in *Scn1a*$^{+/-}$ interneurons were completely rescued by transducing the *Scn1a*-dCas9A system (Ctrl WT, n = 12; Ctrl *Scn1a*$^{+/-}$, n = 10; Scn1a-dCas9A WT, n = 10; *Scn1a*-dCas9A *Scn1a*$^{+/-}$, n = 11; p = 0.02, p = 0.04, 2-way ANOVA followed by Bonferroni's multiple comparisons test) (Figures 6D–6H). Activity clamp confirmed rescue of DS mutant interneuron firing in the face of epileptiform activity following *Scn1a*-dCas9A treatment compared with Ctrl-dCas9A treatment (Ctrl-dCas9A WT, n = 12; Ctrl-dCas9A *Scn1a*$^{+/-}$, n = 10; *Scn1a*-dCas9A WT, n = 10; *Scn1a*-dCas9A *Scn1a*$^{+/-}$, n = 11; p = 0.03, 2-way ANOVA followed by Bonferroni's multiple comparisons test) (Figure 6I). As expected from the molecular data, the increase in excitability in *Scn1a*-dCas9A-treated WT interneurons observed at 9–10 DIV was no longer observed at 18–20 DIV (Figures 6C–6J).

AAV-Mediated *Scn1a*-dCas9A Transduction of Cortical Interneurons Rescues Parvalbumin (PV)+ Interneuron Deficiency and Protects *Scn1a*$^{+/-}$ Mutant Mice from Hyperthermia-Induced Seizures

Given the encouraging results with *Scn1a*-dCas9A treatment obtained on neuronal cultures, we sought to test its efficacy in rescuing the epileptic phenotype in a DS mouse model.

To exploit the *Scn1a*-dCas9A system *in vivo*, we sought to stimulate *Scn1a* expression selectively in forebrain GABAergic interneurons. We used a dual AAV9-based system because these viral particles diffuse efficiently in the brain parenchyma after intracerebroventricular (i.c.v.) injections in neonatal mouse pups.[43] The VP64 activator domain, carrying four tandem copies of VP16, was chosen for *in vivo* delivery because its smaller size allows this dCas9A together with the TRE promoter to fit in an AAV vector. Similar to the aforementioned dual lentiviral system, a second AAV9 was packaged with the sg1P cassette, followed by the *mDlx5/6* promoter driving selective expression of the rtTA-T2A-Tomato cassette in forebrain GABAergic interneurons (Figure 7A).[44,45]

When the *mDlx5/6*-promoter driven dCas9A elements were virally transduced in GAD67-GFP transgenic pups, we estimated that about 85% of the viral reporter tdTomato$^+$ cells in the cerebral cortex also expressed the GFP transgene (Figures S7A–S7C and S7F). Furthermore, different interneuron subtypes could be targeted specifically by our system, as shown by co-labeling of tdTomato with parvalbumin, somatostatin, neuropeptide Y (NPY), or vasoactive intestinal peptide (VIP) (Figures S6B–S6F). Histological characterization of WT litters injected with the dCas9A elements revealed discrete transduction efficiency along the antero-posterior axis, with about 20% of total GABAergic interneurons transduced in cortical areas close to injection sites (Cx1_L, left, and Cx1_R, right; Figure S6G). Neatly, in these same areas, a significant increase in *Scn1a* gene expression was detected in 2-week-old mice treated with the *Scn1a*-dCas9A system compared with the Ctrl-dCas9A system (Figures 7B and 7C). To assess whether *Scn1a*-dCas9A has a functional effect on PV interneurons *in vivo*, we performed patch-clamp analysis on treated *Scn1a*$^{+/+}$ and *Scn1a*$^{+/-}$ mice crossed with PV-Cre;Ai9-tdTomato mice at P21–P28 (Figure S7A).

Current step injections highlighted a decreased frequency-current relationship (Figure S7C) and maximum AP frequency (Figure S7D) in *Scn1a*$^{+/-}$ PV interneurons compared with *Scn1a*$^{+/+}$ when injected with Ctrl-dCas9A. These defects in *Scn1a*$^{+/-}$ PV interneurons were rescued by transducing the *Scn1a*-dCas9A system (*Scn1a*$^{+/+}$;Ctrl-dCas9A, n = 9; *Scn1a*$^{+/-}$;Ctrl-dCas9A, n = 12; *Scn1a*$^{+/-}$;*Scn1a*-dCas9A, n = 11; input/output (I/O), p = 0.003; two-way ANOVA (Figures S7C and S7D).

At 1 month, *Scn1a*$^{+/-}$ mice were implanted with electrodes, and an electroencephalogram (EEG) was recorded after subjecting the mice to hyperthermia-induced seizures. When *Scn1a*$^{+/-}$ mice were exposed to hyperthermia, we observed that the seizure threshold temperature was increased in *Scn1a*-dCas9A- compared with Ctrl-dCas9A-treated mice (Ctrl-dCas9A: 41.93 ± 0.1687, n = 6; *Scn1a*-dCas9A: 42.343 ± 0.1453, n = 6; p = 0.0048, Student's t test) (Figure 7F). Furthermore, *Scn1a*-dCas9A-treated *Scn1a*$^{+/-}$ mice displayed seizures with a generally lower average clinical severity score than Ctrl-dCas9A-treated mice (Ctrl-dCas9A: 5.83 ± 0.17, n = 6; *Scn1a*-dCas9A: 4.83 ± 0.31, n = 6; p = 0.02, chi-square test) (Figure 7G). The average seizure duration defined by EEG recordings was also shorter (Ctrl-dCas9A: 33.5 ± 2.7 s, n = 5; *Scn1a*-dCas9A: 23.9 ± 2.6 s, n = 6; p = 0.029, Student's t test) (Figure 7H). Finally, we observed a non-significant trend for the spike frequency to be lower in *Scn1a*-dCas9A-treated mice compared with Ctrl-dCas9A-treated mice (Figures 7I and 7J).

The upregulation of $Na_v1.1$ during development *in vivo* may be protective against epileptic insults because loss of $Na_v1.1$, in the inverse

n = 15). (E) Histogram of the maximum frequency reached by interneurons during the current step protocol (p = 0.03, Mann-Whitney *U* test). (F) Experimental design of activity clamp in primary neuronal cultures in the presence of 4AP (Materials and Methods). (G and H) Representative full traces (G) and magnified traces (H) for the activity clamp protocol in Ctrl-dCas9A (black trace, sgCtrl) and *Scn1a*-dCas9A (blue trace, sg1P) interneurons. (I) Activity clamp analysis for the number of events during the full traces (left) and cumulative plot for AP frequency (right) (Ctrl, n = 10; *Scn1a*-dCas9A, n = 12; p = 0.0009, unpaired Student's t test).

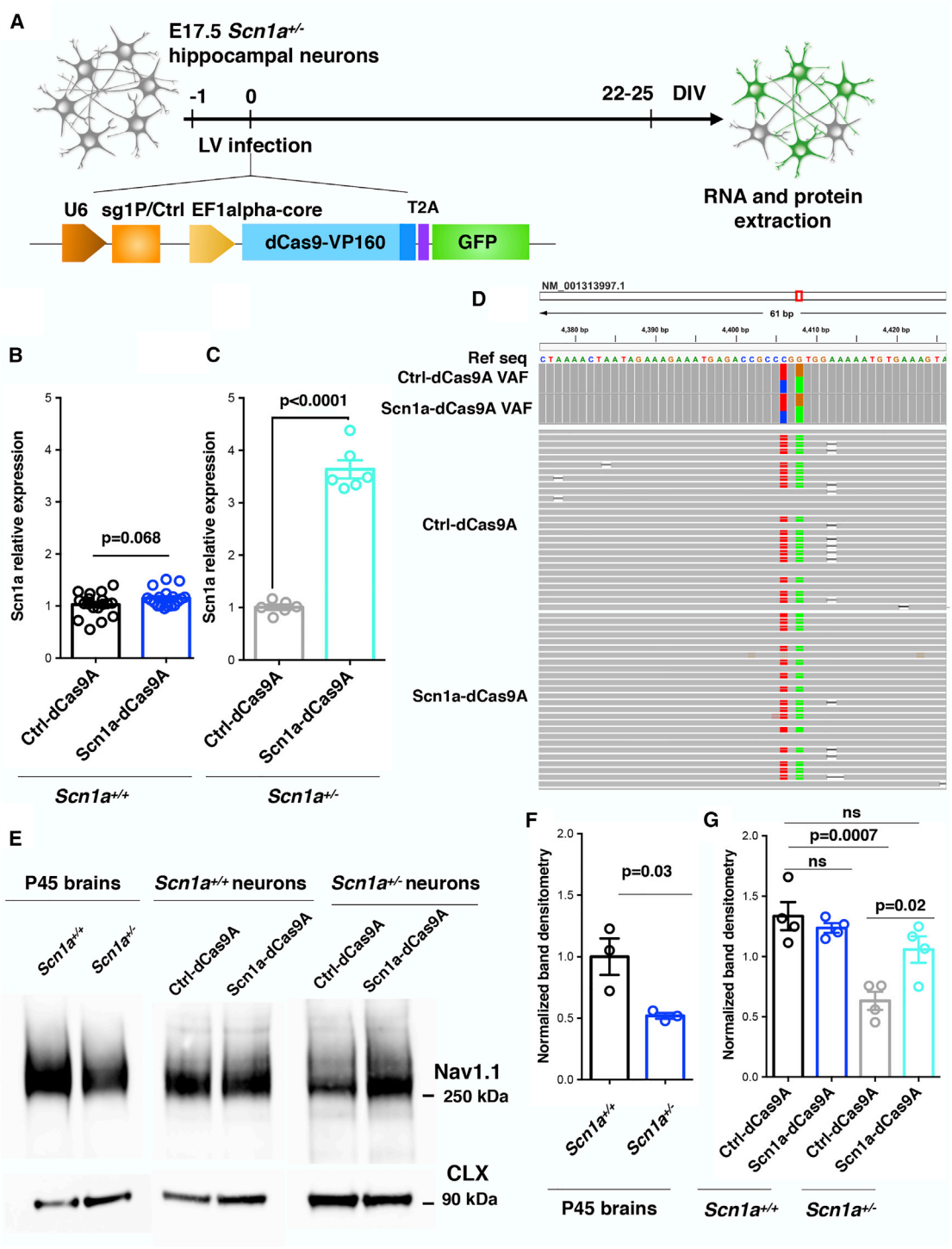

Figure 5. *Scn1a*-dCas9A Stimulates *Scn1a* Basal Expression and $Na_v1.1$ Protein Levels in *Scn1a*$^{+/-}$ Hippocampal Neurons

(A) Schematic drawing of the dCas9A treatments in E17.5 *Scn1a*$^{+/-}$ primary neurons. Neurons were transduced with either the Ctrl-dCas9A or *Scn1a*-dCas9A system 1 day after plating and processed for RNA and protein extraction at 22–25 DIV. (B and C) qRT-PCRs for *Scn1a* transcriptional levels performed on RNA extracted from Ctrl-dCas9A- or *Scn1a*-dCasA-treated *Scn1a*$^{+/+}$(B) and *Scn1a*$^{+/-}$ (C) primary neurons. Plotted data are expressed as relative to Ctrl-dCas9A. *Scn1a*$^{+/+}$: n = 18, p = 0.068; *Scn1a*$^{+/-}$: n = 4, p < 0.0001; Student's t test. (D) Binary alignment map (BAM) within the mouse *Scn1a* transcript (NM_001313997.1). The red box indicates the region amplified and sequenced with high coverage. Ctrl-dCas9A and Scn1a-dCas9A variant allele frequency (VAF) tracks show the observed VAF. Ctrl-dCas9A and

(legend continued on next page)

scenario, is epileptogenic. To test this hypothesis, we performed intraventricular injections of P0 pups with either Ctrl-dCas9A or *Scn1a*-dCas9A viruses using a pan-neuronal promoter. At P14–P17, pups were injected with lipopolysaccharide (LPS) to elicit fever by infection,[46,47] followed by repeated low-dose kainic acid (KA) injections every 30 min 2 h later. Epileptic seizures were scored according to the Racine scale, and pups were observed every 10 min until they reached grade 5, marked by tonic-clonic convulsive seizures (Figure S8A). The time taken to reach grade 5 was used to define susceptibility to epileptic insults. Pups injected with *Scn1a*-dCas9A had a higher seizure threshold compared with sham and Ctrl-dCas9A injected animals, confirming the hypothesis that upregulation of $Na_v1.1$ during development is protective against seizures (Figure S8B).

In conclusion, these results show that the *Scn1a*-dCas9A system can be efficiently delivered *in vivo* by AAV-mediated gene transfer in $Scn1a^{+/-}$ mice to ameliorate temperature-induced seizures characteristic of this DS mouse strain.

DISCUSSION

DS poses severe challenges for developing an effective therapeutic strategy to control epileptic seizures and associated neurodevelopmental dysfunctions. Currently available antiepileptic drugs are inadequate to suppress recurrent seizures. Furthermore, novel gene therapy approaches for *Scn1a* gene replacement are hampered by the relatively large size of the *Scn1a* gene, which exceeds the packaging cargo size of AAV particles. Finally, *Scn1a* transcriptional levels need to be carefully gauged to maintain an $Na_v1.1$ protein level compatible with physiological membrane excitability in mature neurons. In light of these significant hurdles, we propose that the dCas9A-guided approach for *Scn1a* gene regulation has invaluable advantages for developing an effective and safe gene therapy strategy for this disease. We identified the sg1P guide, targeting a sequence close to the *Scn1a* proximal promoter, capable of significantly stimulating *Scn1a* expression. A preliminary genomic analysis confirmed that this promoter region is transcriptionally active in the adult mouse and human neurons, showing the exact transcriptional start site (TSS) by CAGE-seq and the crucial epigenetic modifications associated with its functional state. Rapid advances regarding our knowledge of the transcriptional and epigenetic state of the regulatory elements across the genome of neurons will improve the design of effective guides. Importantly, our data provide evidence that this dCas9-based activation system can further stimulate *Scn1a*, increasing its basal expression in young post-mitotic neurons. Surprisingly, we could not detect a significant increase in *Scn1a* expression in mature WT neurons, whereas it was evident in $Scn1a^{+/-}$ neurons at both the mRNA and protein levels upon *Scn1a*-dCas9A treatment. Considering that approximately 70% of the newly synthesized $Na_v1.1$ constitutes a metabolically stable intracellular pool of protein and only 30% is trafficked to the plasma membrane and axon initiation segment (AIS),[48] we can speculate that excessive accumulation of $Na_v1.1$ induces negative regulation of the *Scn1a* transcript that cannot be overcome even by *Scn1a*-dCas9A treatment in a WT situation. Conversely under $Scn1a^{+/-}$ conditions, only half of the protein is produced, and this "saturation" is not achieved. In light of this, we propose that the total amount of $Na_v1.1$ channel available in the cell can exert control by repressing transcription or destabilizing *Scn1a* mRNA. Further studies are required to determine the details of this regulation and to assess whether stimulation of *Scn1a* gene expression alters the chromatin marks within the promoter region with specific histone modifications associated with this particular transcriptional state. These results have valuable implications for manipulation of gene expression in the adult brain, providing a tool for targeted and tunable transcriptional regulation of potentially any genetic element. We achieved good gene transcriptional activation using dCas9 fused with the effector domain VP64 or VP160. However, recent studies have identified novel transactivators that can elicit higher levels of gene activation.[29,34,49] Establishment of different Cas9 activator systems, each with its own advantages, can provide an invaluable toolbox for obtaining the right fine-tuning of transcriptional levels adequate for each specific application. Using global RNA-seq, we showed that targeted *Scn1a* gene activation was exquisitely specific, with no detectable off-target gene activation in primary neurons. These data reveal the high specificity of this approach, which will contribute to the high safety level for its future therapeutic applications. In fact, both the new models for accurate prediction of sgRNA off-targets and the strict requirement for targeting promoter regions close to the TSS contribute to elevating the level of specificity of this approach. Additionally, use of dCas9 eliminates the risks of DNA cleavage and its consequences in post-mitotic neurons that have lost the ability to activate homology-directed repair mechanisms to resolve DNA damage.[50,51] Importantly, dCas9-based stimulation of *Scn1a* expression led to a significant increase in membrane-associated $Na_v1.1$ protein levels that restored correct functioning of DS mutant inhibitory interneurons *in vitro*. Our approach did not distinguish between the two *Scn1a* alleles and also stimulated expression of the mutant *Scn1a* allele (R1407X). Multiple studies have confirmed that the great majority of *SCN1A* mutations are loss-of-function ones and have a negligible effect because they do not produce any stable protein capable of functioning at the neuronal membrane.[10] However, few mutations in *SCN1A* have been hypothesized from *in vitro* studies to cause the disease through a gain-of-function mechanism.[52] We anticipate that, in these particular cases, our

Scn1a-dCas9A read tracks display a sample of about 30 different sequencing reads per sample; nucleotides diverging from the reference genome are highlighted. (E) Western blot for $Na_v1.1$ and Calnexin on protein lysates from adult (P45) $Scn1a^{+/+}$ and $Scn1a^{+/-}$ mice (left panel) and from Ctrl-dCas9A- and *Scn1a*-dCasA-treated $Scn1a^{+/+}$ and $Scn1a^{+/-}$ neurons at 22–25 DIV (center and right panels). (F) Densitometric quantification of immunoreactive bands in the western blots of adult mouse brains. Values corresponding to the $Na_v1.1$ band were normalized to Calnexin levels (n = 3, p = 0.03, Student's t test). (G) Densitometric quantification of immunoreactive bands in the western blots of $Scn1a^{+/+}$ and $Scn1a^{+/-}$ neurons transduced with Ctrl-and *Scn1a*-dCas9A.Values corresponding to the $Na_v1.1$ band were normalized to Calnexin levels (n = 4, one-way ANOVA followed by Turkey's multiple comparisons test). Data are shown as mean ± SEM, with dots representing individual samples.

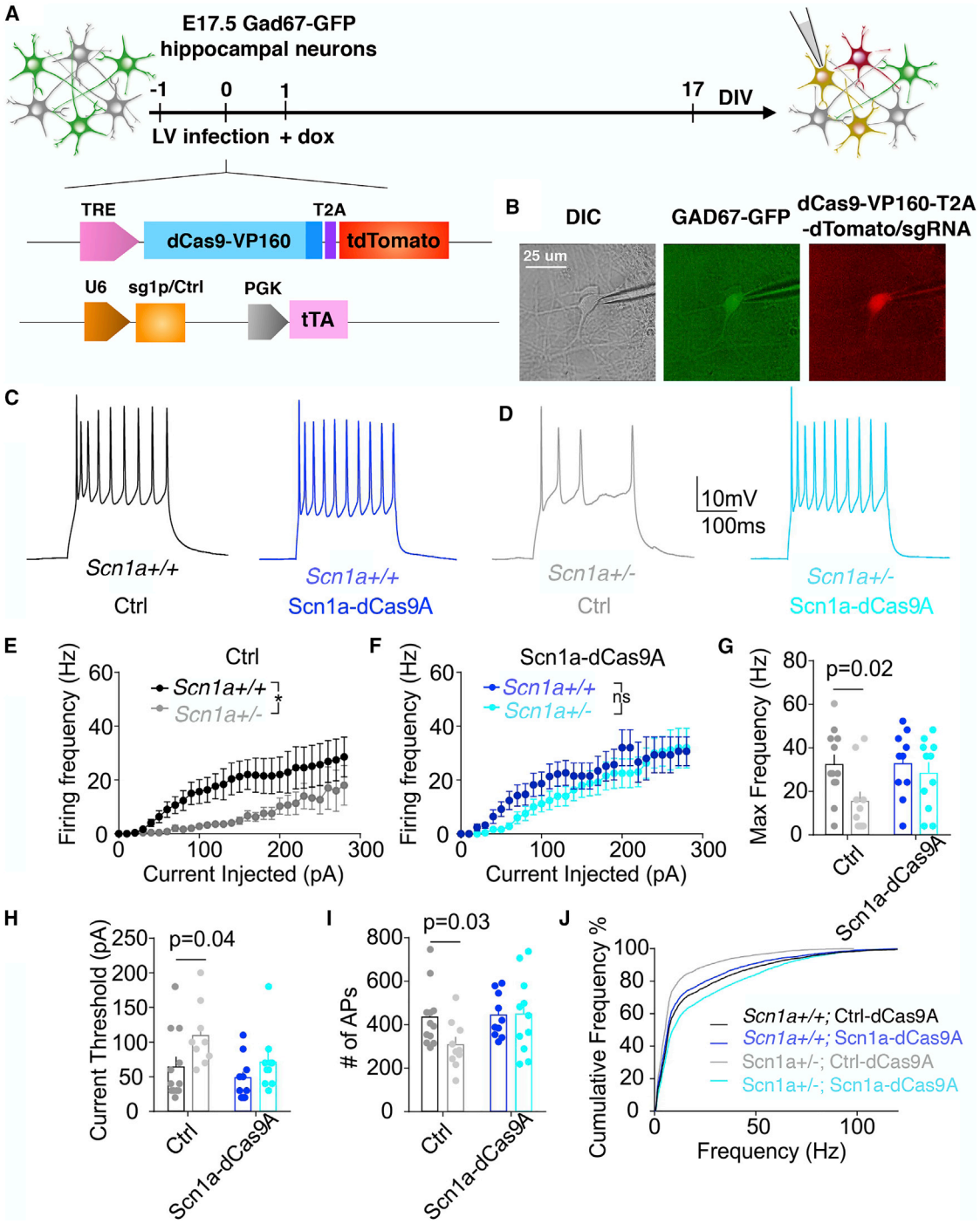

Figure 6. *Scn1a*-dCas9A Rescues Neuronal Excitability Defects in Cortical Mature *Scn1a*$^{+/-}$ Interneurons

(A) Schematic drawing showing the experimental time frame for lentiviral transductions and functional analysis of *Scn1a*$^{+/+}$;GAD67-GFP^{+} or *Scn1a*$^{+/-}$;GAD67-GFP^{+} primary hippocampal neurons transduced with the two depicted lentiviruses. (B) Representative images of a patch-clamp-recorded *Scn1a*$^{+/-}$ interneuron expressing both GFP under the GAD67 promoter and tdTomato reflecting the active *Scn1a*-dCas9A system (Materials and Methods). (C and D) Representative current-clamp traces of APs induced by single current steps administered to Ctrl-dCas9A-transduced WT interneurons (black trace, C), *Scn1a*-dCas9A-transduced *Scn1a*$^{+/+}$interneurons (blue trace, C), Ctrl-dCas9A-transduced *Scn1a*$^{+/-}$ interneurons (gray trace, D), and *Scn1a*-dCas9A-transduced *Scn1a*$^{+/-}$ interneurons (cyan trace, D). (E and F) Firing

(legend continued on next page)

approach would not be of any advantage. Neuropathological studies have shown that, even in advanced stages of the disease, there is no evident sign of neuronal cell loss in patients.[53] These observations strongly imply that dysfunctional interneurons can potentially recover their activity whenever a sufficient amount of $Na_v1.1$ channel is available and indicate that at least some DS pathological defects are reversible. Altogether, these results raise the prospect of a cure for this disease even when pathological manifestations are already evident.

In this study, the different elements of the dCas9 activation system were packaged in two different AAVs but designed to provide interdependent expression of the different genetic elements. Considering that DS globally affects forebrain interneurons, we carried out AAV i.c.v. injections in neonatal mouse pups to cover the entire forebrain structures with a single treatment. In patients, because symptom onset generally occurs within the first two years of life and some more time is required to ascertain *Scn1a* gene mutation by exon sequencing, later delivery of gene therapy will be required. Nevertheless, the recent discovery of new AAV synthetic serotypes capable of crossing the blood-brain barrier from the bloodstream might open new opportunities for delivery of therapeutic AAVs for treating CNS disorders. In this respect, peripheral injections of AAV9 in infants with spinal muscular atrophy (SMA), a devastating infantile neurological disorder affecting spinal motor neurons, have recently shown substantial and long-term clinical benefits.[54] In fact, a single intravenous infusion of the AAV9 expressing the corrected gene resulted in wide protection of motor skills for an extensive period of time and longer survival.[54] This unprecedented clinical success regarding SMA with a systemic AAV gene therapy approach might facilitate the introduction of a similar strategy to treat other incurable neurological infantile disorders and DS in particular.

Our gene therapy strategy was targeted selectively to forebrain interneurons using the small *Dlx5/6* enhancer, which has been shown to reliably deliver reporter genes within these neuronal classes.[44,45] Similarly, we reported that this regulatory element also ensured restricted expression of the transgenes in the GAD67-GFP neuronal sub-population in DS adult mice. Even though *Scn1a* is also expressed in subpopulations of cortical excitatory neurons, our strategy almost completely avoided *Scn1a* gene activation in these cells. Nevertheless, *Scn1a* deletion in this neuronal population does not induce noticeable abnormalities in mice, whereas it ameliorates the pathological phenotype of mice with *Scn1a* deletion in GABAergic neurons.[13] *Scn1a* expression levels are likely different in cortical excitatory and inhibitory neurons, and our approach does not allow us to deliver different levels of gene activation in different neuronal subtypes. Thus, we considered it safer to employ the *Dlx5/6* enhancer to exclusively target the neuronal population, whose dysfunction leads to pathological manifestations. The possibility that transduction of extra-cortical interneurons may affect treatment efficacy needs to be considered. Alternatively, a more selective promoter driving expression of the *Scn1a*-dCas9A system only in cortical interneurons and not in other interneurons (i.e., striatal) could be exploited. The *Scn1a* gene activation system attenuated induced epileptic seizures in terms of threshold temperature, total duration, overall clinical severity, and recovery period. However, seizures were not completely suppressed. The results can be explained by the relatively low co-infection efficiency of the two separate AAVs in the interneuron population, reaching around 20% in the injected area. In fact, the considerable size of SpCas9 requires use of two independent AAVs to assemble all elements of the activation system. Thus, future work is necessary to improve this strategy to package all of the system in a unique AAV vector by using significantly smaller Cas9 orthologs, such as SaCas9,[55] GeoCas9,[56] CjCas9.[57] When the AAV vector for *Scn1a*-dCas9A treatment is optimized, it would be interesting to also test its effect on the survival rate and spontaneous seizure number and severity in Dravet mice. In conclusion, we showed that the dCas9 activation system can be tailored to obtain a robust and highly specific activation of the *Scn1a* gene both in cultured neurons and in brain tissue. Moreover, the dCas9 activation system can be packaged into AAVs to establish a gene therapy approach for treating DS mice and obtaining protection from temperature-induced epileptic seizures. A similar approach can then be considered for other haploinsufficient genetic disorders where stimulation of the WT allele can rescue molecular dysfunction and lead to a clinical benefit.

MATERIALS AND METHODS

Bioinformatics Analysis

Transcriptomics and epigenetics next-generation sequencing (NGS) data were downloaded from the ENCODE[58] and Functional Annotation of the Mammalian Genome (FANTOM)[59] databases. Tracks are visualized along the mm10 mouse reference genome with the Integrative Genome Viewer (IGV).[60]

Molecular Cloning

sgRNAs were cloned in a LV-U6 vector as described previously. Ef1alpha-dCas9VP160-T2A- PuroR was generated from pAC94-pmax-dCas9VP160-2A-puro, a gift from R. Jaenisch (Addgene plasmid 48226).[61] The dCas9VP160-2A-puro cassette was cut with AgeI and inserted into the TetO-FUW vector digested with AgeI. The dCas9VP160-2A-puro cassette was restriction digested with HpaI/AfeI and blunt-cloned into the Ef1alpha-GFP promoter, where GFP was removed by SmaI/EcoRV digestion. Ef1alpha-dCas9VP160-T2A-GFP was obtained by restriction digestion of Ef1alpha-dCas9VP160-T2A-PuroR with AscI/XbaI; the VP160-T2A fragment was obtained by AscI/XhoI digestion from Ef1alpha-dCas9VP160-T2A-Puro^R, whereas the GFP fragment was PCR amplified with

frequency versus injected current for Ctrl-dCas9A-transduced (E) and *Scn1a*-dCas9A-transduced (F) *Scn1a*$^{+/+}$ and *Scn1a*$^{+/-}$ interneurons. Ctrl-dCas9A wild-type, n = 12; Ctrl-dCas9A *Scn1a*$^{+/-}$, n = 10; *Scn1a*-dCas9A wild-type, n = 10; *Scn1a*-dCas9A *Scn1a*$^{+/-}$, n = 1 ($p < 0.05$, 2-way ANOVA). (G and H), Histogram plots of the maximum frequency (G) and current threshold (H) reached by interneurons during the current step protocol ($p = 0.02$, $p = 0.04$, 2-way ANOVA/Bonferroni's multiple comparisons tests). (I and J) Activity clamp analysis for the number of events during the full traces (I) and cumulative plot for AP frequency (J) ($p = 0.03$, 2-way ANOVA/Bonferroni's multiple comparisons tests).

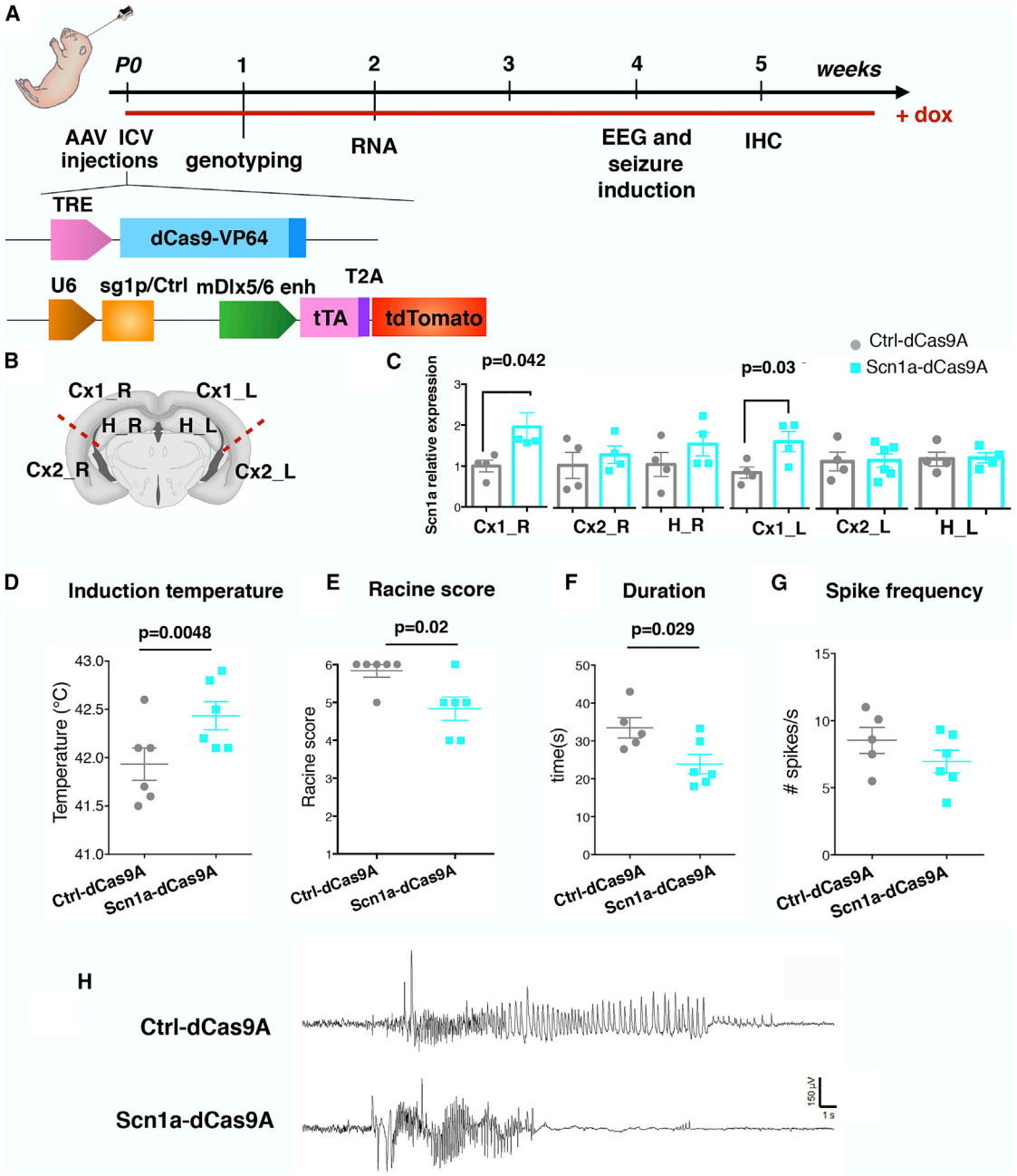

Figure 7. *In Vivo Scn1a*-dCas9A Delivery through Intracerebroventricular Brain Injections Attenuates Seizures in the *Scn1a*$^{+/-}$ Mice

(A) Schematic illustration showing the experimental setting for *in vivo* delivery of the *Scn1a*-dCas9A system through intracerebroventricular injections into P0 pups of AAVs (2.9) carrying the Ctrl-dCas9A and *Scn1a*-dCas9A system. After 1 week, treated mice were genotyped, and then *Scn1a*$^{+/-}$ animals then selected for implantation of EEG electrodes and analysis of the epileptic phenotype. Wild-type (WT) litters were processed for molecular (2 weeks) and histological (5 weeks) characterization of *in vivo* AAV targeting. Doxycycline (dox) was administered in drinking water or food until final analysis. (B) Scheme of cerebral cortex dissection in treated mice for *Scn1a* expression at the mRNA level (Cx1, medial cortex; Cx2, lateral cortex; R, right; L, left). (C) qRT-PCRs performed on dissected areas of the brains in Ctrl-dCas9A- and *Scn1a*-dCas9A-treated wild-type mice (n = 6 for each group, p = 0.042 for Cx1_R, p = 0.03 for Cx1_L, Student's t test). (D and E) Mean (± SEM) threshold temperatures (D) for the occurrence of myoclonic seizures (n = 6 for each group, p = 0.048, Student's t test) and severity of the epileptic seizures, evaluated by a modified Racine score (E) in Ctrl-dCas9A-and *Scn1a*-dCas9A-treated *Scn1a*$^{+/-}$ mice (n = 6 for each group, p = 0.02, chi-square test). (F and G) Duration (F) and spike frequency (G) of temperature-induced seizures in Ctrl-dCas9A-or *Scn1a*-dCas9A-treated *Scn1a*$^{+/-}$ mice (n = 5 for Ctrl-dCas9A and n = 6 for *Scn1a*-dCas9A treated mice, p = 0.029 for duration and p = 0.2 for spike frequency, Student's t test). (H) Representative EEG traces of hyperthermia-induced seizures in Ctrl-dCas9A-and *Scn1a*-dCas9A-treated *Scn1a*$^{+/-}$ mice.

primers containing XhoI/XbaI restriction sites; the vector and the two fragments were ligated together.

LV-TRE-dCas9VP160-T2A-tdTomato was obtained from TetO-FUW dCas9VP160-2A-puro digested with AscI/XbaI; the VP160-T2A fragment was obtained by AscI/XhoI digestion from Ef1alpha-dCas9VP160-T2A-Puro^{R}, whereas the tdTomato fragment was PCR amplified with primers containing XhoI/XbaI restriction sites; the vector and the two fragments were ligated together. The LV-sgRNA-hPGK-rtTA vector was obtained by digesting LV-U6-sgRNA with BamHI and cloning rtTA fragment BamHI digested from LV-hPGK-rtTA. The intermediate LV-U6-rtTA was ClaI-XhoI digested, and the PGK promoter was PCR amplified with primers with ClaI/XhoI and then cloned. AAV-TRE-dCas9-VP64 was obtained by restriction digestion of AAV-SpCas9 (a kind gift from F. Zhang, Addgene PX551),[51] where the Mecp2 promoter was removed by XbaI/AgeI digestion and the TRE promoter was amplified with the following primers: FW XbaI (5′-GCTCTAGACCAG TTTGGTTAGATCTC-3′) and RV AgeI (5′-GCACCGGTGCGATC TGACGGTTCACT-3′). SpCas9 was removed with AgeI/EcoRI and Cas9m4-VP64 (a kind gift from G. Church, Addgene 47319)[26] was digested with AgeI EcoRI. The VP64 fragment was PCR amplified with the following primers with EcoRI sites: FW: 5′-GATCATCGAGC AAATAAGCGAATTCTC-3′ and RV: 5′-gctaaGAATTCTTATCTA GAGTTAATCAGCATG-3′.

Virus Production

LVs were produced as described previously.[62] For AAV production, replication- incompetent, recombinant viral particles were produced in 293T cells by polyethylenimine (PEI) (Polyscience) co-transfection of three different plasmids: a transgene-containing plasmid, a packaging plasmid for rep and cap genes, and pAdDeltaF6 for the three adenoviral helper genes. The cells and supernatant were harvested at 120 h. Cells were lysed in Tris buffer (50 mM Tris (pH 8.5), and 150 mM NaCl; Sigma-Aldrich) by repetitive freezing-thawing cycles (3 times), lysed in Tris buffer, and combined with correspondent cell lysates. To clarify the lysate, benzonase treatment was performed (250 U/mL, 37°C for 30 min; Sigma-Aldrich) in the presence of 1 mM $MgCl_2$ (Sigma-Aldrich), and cellular debris was separated by centrifugation (2,000 × *g*, 30 min). The viral phase was isolated by an iodixanol step gradient (15%, 25%, 40%, and 60% Optiprep; Sigma-Aldrich) in the 40% fraction and concentrated in PBS with a 100,000 molecular weight cutoff concentrator (Vivaspin 20, Sartorius Stedim). Virus titers were determined by measuring the number of DNase I-resistant viral particles, using qPCR with a linearized genome plasmid as a standard. TRE-dCas9-VP64 was produced by VectorBuilder (CA, USA).

Mice

Mice were maintained at the San Raffaele Scientific Institute institutional mouse facility (Milan, Italy). *Scn1a*$^{+/-10}$ mice were backcrossed with 129Sv mice, whereas GAD67-GFP,[63] *Pvalb*$^{tm1(cre)Arbr}$ (JAX 017320, PV-Cre), and Rosa26$^{LSL\text{-}tdTomato}$ (JAX 007909, Ai9) mice were backcrossed with C57BL/6N mice. PV-Cre$^{+/+}$ mice were crossed to Ai9$^{+/+}$ mice to generate PV-Cre$^{+/+}$ Ai9$^{+/+}$ mice. Those mice were then crossed with 129Sv.Scn1a$^{+/-}$ mice to generate Scn1a $^{+/-}$;PV-Cre$^{+/-}$ Ai9$^{+/-}$ mice and Scn1a$^{+/-}$;PV-Cre$^{+/-}$ Ai9$^{+/-}$. All procedures were performed according to protocols approved by the internal institutional animal care and use committee (IACUC) and reported to the Italian Ministry of Health according to European Commission Council Directive 2010/63/EU and in accordance with the UK Animals (Scientific Procedures) Act of 1986.

Cell Cultures and Primary Neuron Derivation

P19 cells were cultured in alpha-MEM (Sigma-Aldrich) supplemented with 10% fetal bovine serum (Sigma- Aldrich), 1% non-essential amino acids (Gibco), 1% sodium pyruvate (Sigma-Aldrich), 1% glutamine (Sigma-Aldrich), and 1% penicillin/streptomycin (Sigma-Aldrich). Cells were split every 2–3 days using 0.25% trypsin (Sigma-Aldrich). For transfection, Lipofectamine 300 (Thermo Fisher Scientific) was used according to the manufacturer's protocol. Primary cultures of mouse embryonic hippocampal neurons were prepared from embryonic day 17.5 (E17.5) embryos or P0 pups derived from GAD67-GFP knockin and *Scn1a*$^{+/-}$;GAD67-GFP pregnant females. In the latter case, each brain was processed separately, and a skin biopsy was used for genotyping. Briefly, after dissection, hippocampi were enzymatically digested with 0.025% trypsin (Gibco) in Hank's balanced salt solution (HBSS; Euroclone) for 20 min at 37°C.Then HBSS with trypsin was removed, and the hippocampi were washed with plating medium (neurobasal medium [Gibco] supplemented with 2% B27, 3.3 mM glucose, 1% glutamine, and penicillin/streptomycin) and mechanically dissociated with a P1000 pipette to obtain a homogeneous cell suspension. Cells were then plated on plates coated with poly-L-lysine (PLL; 0.1 mg/mL) and coverslips. LV infection was performed at DIV 1, and neurons were used at DIV 10 or 21 for electrophysiology, western blot analysis, and immunofluorescence. For recordings from interneurons, we patched cells that showed co-localization of both green (indicating interneurons) and red (indicating successful lentiviral transduction) fluorescent signals.

Western Blotting

Total cerebral cortices from *Scn1a*$^{+/-}$ mice, WT mice, and primary neurons were homogenized using the Mem-PER Plus Membrane Protein Extraction Kit (Thermo Fisher Scientific) according to the manufacturer's instructions to enrich for the membrane-bound proteins. Western blot analysis was performed on Nupage 4%–12% gradient gels (Thermo Fisher Scientific) using primary antibodies against the following proteins: anti-$Na_v1.1$ (1:200, Millipore) and anti-Calnexin (1:5,000, Sigma).

RNA Isolation qRT-PCR

RNA was extracted using TRI reagent (Merck) according to the manufacturer's instructions. For qRT-PCR, cDNA synthesis was obtained using the ImProm-II Reverse Transcription System (Promega), and then qRT-PCR was performed in triplicate with custom-designed oligos (Table S2) using Titan HotTaq EvaGreen qPCR Mix (no ROX)

(BIOATLAS). Analysis of relative expression was performed using the ΔΔCt method.

RNA-Seq

RNA libraries were generated starting from 1 μg of total RNA extracted from Ctrl-dCas9A and *Scn1a*-dCas9A neurons. RNA quality was assessed by using a Tape Station instrument (Agilent). To avoid over-representation of 3′ ends, only high-quality RNA with a RNA integrity number (RIN) of 8 or higher was used. RNA was processed according to the QuantSeq 3′ mRNA-Seq Library Prep Kit protocol. The libraries were sequenced on an Illumina HiSeq 2500 with 50-bp stranded reads using Illumina TruSeq technology. Image processing and basecall were performed using the Illumina real-time analysis software. Fastq files were aligned to the mouse genome (NCBI37/mm9) with Bowtie2.[64] Differential gene expression and functional enrichment analyses were performed with DESeq2.[65]. Statistical analysis was performed with the SPSS statistical package (IBM). Data were deposited in NCBI GEO: GSE111436.

Deep Sequencing Data Analysis

Indexed paired-end libraries were generated starting from 1 μg of PCR amplicon spanning the $Scn1a^{RX}$ gene mutation[10] performed on cDNA obtained from RT RNA using Illumina TruSeq Nano DNA Library Prep Kits according to the manufacturer's instructions. Libraries were sequenced on an Illumina MiSeq. FASTQ reads were aligned to the hg38 human reference genome with Bowtie2. Alignments were visualized and quantified with the IGV genome browser.

In Vitro Electrophysiology

Current Steps

For current-clamp recordings, the internal solution contained 126 mM K-gluconate, 4 mM NaCl, 1 mM $MgSO_4$, 0.02 mM $CaCl_2$, 0.1 mM 1,2-bis(2-aminophenoxy)ethane-N,N,N′,N′-tetraacetic acid (BAPTA), 15 mM glucose, 5 mM 4-(2-hydroxyethyl)-1-piperazineethanesulfonic acid (HEPES), 3 mM ATP-Na_2, and 0.1 mM GTP-Na (pH 7.3). The extracellular (bath) solution contained 2 mM $CaCl_2$, 140 mM NaCl, 1 mM $MgCl_2$, 10 mM HEPES, 4 mM KCl, and 10 mM glucose (pH 7.3). D-(−)-2-amino-5-phosphonopentanoic acid (D-AP5; 50 μM), 6-cyano-7-nitroquinoxaline-2,3-dione (CNQX; 10 μM), and picrotoxin (PTX; 30 μM) were added to block synaptic transmission. Experiments were performed at room temperature (22°C–24°C). Transduced cortical and hippocampal interneurons were identified because of GAD67-GFP and tdTomato (dCas9A system) expression. Neurons with unstable resting potential (or more than −50 mV), bridge balance of more than 15 MΩ, and/or holding current of more than 200 pA at −70 mV were discarded. Bridge balance compensation was applied, and the resting membrane potential was held at −70 mV. Current step protocols were used to evoke APs, injecting 250-ms-long depolarizing current steps of increasing amplitude (Δ 10 pA, max 280 pA). Recordings were acquired using a Multiclamp 700A amplifier (Axon Instruments, Molecular Devices) and a Power3 1401 (Cambridge Electron Design [CED]) interface combined with Signal software (CED), filtered at 10 kHz, and digitized at 50 kHz. Passive properties were calculated from the hyperpolarizing steps of the current-clamp step protocol. Input resistance is an average of three steps (2 negative and 1 positive) and is defined as the as ΔV/I. Capacitance was calculated in the current-clamp hyperpolarizing step as follows. First, the resistance was determined as voltage derivative (dV)/DI (voltage/current), and then the cell time constant (tau) was obtained, fitting the voltage changing between baseline and hyperpolarizing plateau. Capacitance was calculated as tau/resistance. Capacitance is the time constant of the voltage between the baseline and the plateau during a hyperpolarizing step. Single AP parameters were calculated as described previously.[62] An event was detected as an AP when cross 0 mV and when the rising slope was more than 20 mV/ms in a range of injected current from 0 pA to 500 pA. All recordings and analyses were carried out blinded to the transduced vector.

Activity Clamp

For activity clamp experiments, current traces in voltage-clamp configuration in the presence of 4AP were recorded, holding GFP-positive interneurons (18 DIV) at −70 mV in the presence of $GABA_A$ and N-methyl-D-aspartate (NMDA) blockers. The resulting AMPA current traces were converted in conductance (G = I/V). Using Signal dynamic clamp software in conjunction with CED Power 1401-3 (CED), the conductance traces were used to inject currents into interneurons in current-clamp configuration. During recordings, the voltage of the patched neurons was read in real time and used to calculate the current to be injected from the 4AP conductance trace. To compare different cells, the conductance threshold was calculated in each neuron prior to each dynamic clamp experiment. For voltage-clamp spontaneous excitatory synaptic activity of the epileptic traces (4AP, 100 μM) and current-clamp recordings in dynamic clamp configuration, the internal and extracellular solutions were the same as described above for neuronal whole-cell patch-clamp recordings. For voltage-clamp recordings in the extracellular solution, D-AP5 (50 μM) and PTX (30 μM) were added to block $GABA_A$ and NMDA receptors, respectively. For current-clamp recordings, D-AP5 (50 μM), CNQX (10 μM), and PTX (30 μM) were added to block NMDA receptors, AMPA receptors, and $GABA_A$ receptors, respectively. Experiments were performed at room temperature (22°C–24°C). For voltage-clamp recordings, neurons with unstable resting potential and/or a leak current of more than 100 pA were discarded, and neurons were clamped at −70 mV. For current-clamp recordings, neurons with unstable resting potential and/or a bridge balance of more than 15 MΩ were discarded. Bridge balance compensation was applied, and the resting membrane potential was held at −70 mV. An AMPA conductance step protocol (Erev = 0 mV; τ = 1 ms; ΔG = 1 nS) was used to find the conductance threshold that elicited an AP, and then the epileptic conductance trace was scaled to the 15% of the conductance threshold. Neurons that were unable to generate at least one AP were therefore excluded. The sampling frequencies in voltage- and current-clamp configuration were set at 20 kHz to perfectly overlap the conductance traces with the software voltage reading. To analyze the dynamic clamp traces, an automatic MATLAB script was used[41] to detect events and calculate APs parameters. An event was selected as an AP

when its peak crossed 0 mV and its dV/time derivative (dt) was more than 20. Voltage threshold was calculated as the first point with a derivative of more than 20 V/s. All recordings and analyses were carried out blinded to the transduced vector. Recordings were acquired using a Multiclamp 700A amplifier (Axon Instruments, Molecular Devices, Sunnyvale, CA, USA) and Signal dynamic clamp software in conjunction with CED Power 1401-3 (CED, Cambridge Electronic Design), filtered at 10 kHz, and digitized at 50 kHz.

Ex Vivo Electrophysiology

Mice were sacrificed after deep isoflurane anesthesia, and brains were extracted. 350-μm-thick coronal sections were cut using a Leica VTS 1000 vibratome. After the cut, the slices were allowed to recover for 30 min at 32°C in modified artificial cerebrospinal fluid (ACSF) containing 92 mM sucrose, 87 mM NaCl, 2.5 mM KCl, 1.25 mM NaH_2PO_4, 25 mM $NaHCO_3$, 25 mM glucose, and 10 mM $MgSO_4$ aerated with 95% O_2 and 5% CO_2 (pH 7.4); slices were then allowed to recover at room temperature for at least 45 min before recording.

Current-clamp recordings were performed using a MultiClamp 700B amplifier (Molecular Devices) with pCLAMP 10 software. Pipette capacitance and resistance were always compensated. Signals were low-pass-filtered at 10 kHz and sampled at 50–100 kHz; the signal was digitized using a Digidata 1550 D/A converter (Molecular Devices).

Cells were held at 30°C–32°C. The extracellular solution contained 125 mM NaCl, 25 mM NaHCO3, 2 mM CaCl2, 2.5 mM KCl, 1.25 mM NaH_2PO_4, 1 mM $MgSO_4$, and 10 mM D-glucose aerated with 95% O_2 and 5% CO_2 (pH 7.4). The patch pipette contained 124 mM KH_2PO_4, 5 mM KCl, 2 mM $MgCl_2$, 10 mM NaCl, 10 mM HEPES, 0.5 mM EGTA, 2 mM Na-ATP, and 0.2 mM Na-GTP (pH 7.25, adjusted with KOH).

Ctrl-and *Scn1a*-dCas9A PV^+ interneurons were identified via tdTomato and GFP expression visualized with epifluorescence microscopy. The input/output relationship was determined by plotting AP frequency in response to progressive 500-ms, 50-pA current step injection. An AP was defined as spikes having a rising slope of more than 20 V/s and an amplitude exceeding −15 mV. Maximal steady-state firing frequency was defined as the maximal mean firing frequency in response to a current injection. Input resistance (Rm) was calculated from a −50 pA step from the resting membrane potential. AP amplitude was calculated from the AP threshold, defined as the voltage at which the first derivative (dV/dt) of the AP waveform reached 10 mV/ms, to the absolute value of the AP peak for the first spike obtained at the rheobase (defined as the minimal current injection able to elicit neuronal firing, determined through 10-pA current steps). Spike width was determined at half-amplitude (half-width) between the AP threshold and peak. Spike frequency adaptation (SFA) was calculated as the ratio of the first to the 10^{th} inter-spike interval (ISI1/ISI10). Maximal rise and decay slope were defined, respectively, as the maximal and minimal value of the first derivative of the AP waveform.

Intracerebroventricular Injections

Neonatal mice were anesthetized in ice for 3 min. 5 μl of viral suspension containing two AAVs (titer, 10^{13} viral genomes [vg]/mL) (TRE-dCas9-VP64 and pU6-sgCrtl/sg1P-mDlx5enh-rtTa-T2A-Tomato/GFP, 1:1), and 0.05% Fast Green FCF (Sigma Aldrich) was injected into lateral ventricles using a Hamilton syringe with a 33G needle. After injections, pups were placed on a warming pad until they regained normal color and movement. Subsequently, they were rubbed with bedding to prevent rejection before reintroducing the mother into the cage. Dox was administered immediately in drinking water or food. One week after the injections, mice were genotyped.

Immunostaining

Cells and neurons were fixed in ice-cold 4% paraformaldehyde (PFA) in phosphate buffer (PB) for 20 min. Mice were anesthetized with ketamine/xylazine and t perfused with 0.1 M PB at room temperature at pH 7.4 with freshly prepared PFA in PB. Tissues were post-fixed in 4% PFA overnight and then soaked in cryoprotective solution (30% sucrose in PBS). Tissues were sectioned using a cryostat after optimal cutting temperature (OCT) compound embedding in dry ice. For immunofluorescence, free-floating, 30-μm-thick coronal sections or plated cells were rinsed in PBS and incubated for 20 min with 2% Triton X-100, and 3% BSA for 1 h was used to saturate the nonspecific binding site before overnight incubation with the primary antibody (diluted in a solution containing 1% BSA and Triton X-100 at room temperature). Following incubation, sections were rinsed three times in PBS and incubated for 1 h with the secondary antibody.

Primary antibodies for the following epitopes were used: red fluorescent protein (RFP) (rabbit, 1:500, MBL International), GFP (chicken, 1:500, Molecular Probes), Calbindin (mouse, 1:200, Swant), PV (mouse, 1:500, Swant), somatostatin (SST) (rat, 1:200, Millipore), NPY (rabbit, 1:500, Immunostar), VIP (rabbit, 1:500, Immunostar), Map2 (mouse, 1:250, Immunological Science), GABA (rabbit, 1:1,000, Sigma-Aldrich). Slices and cell coverslips were mounted with fluorescent mounting medium (Dako). Images were captured with a Nikon Eclipse 600 fluorescence microscope.

Surgery for Electrode Implantation, Seizure Induction, and EEG

At least 5 days before recordings, epidural stainless steel screw electrodes (0.9 mm in diameter and 3 mm long) were surgically implanted under intraperitoneal anesthesia (100 mg/kg ketamine, 10 mg/kg xylazine) and secured using dental cement (Ketac Cem, ESPE Dental, Seefeld, Germany). Two active electrodes were placed on the right and left parietal areas (2 mm lateral to the midline, 1 mm posterior to the bregma) and one over the occipital area (1 mm posterior to lambda) as a common reference.

For video EEG recording, the implanted electrodes were connected via flexible cables to an amplifier, and the EEG signal was sampled at 256 Hz, coded with 16 bits, and digitally saved using a System Plus device (Micromed, Mogliano Veneto, Italy). To obtain a good signal-to-noise ratio for seizure display, after acquisition, EEG traces were bandpass-filtered between 0.3 and 10 Hz. Video EEG recordings

were inspected to detect seizures, defined as high-amplitude (at least twice the baseline) rhythmic discharges lasting at least 5 s. We defined the beginning of the seizure as the first EEG change; the end of the seizure was defined as the end of ictal EEG activity.

To induce seizures, we adopted a protocol modified from Oakley et al.[16] Mice were placed in a glass beaker and heated with an infrared heat lamp (HL-1, Phisitemp, Clifton, New Jersey) controlled by a TCAT-2DF thermocontroller (Phisitemp, Clifton, New Jersey). Mouse rectal temperature was continuously monitored with a RET-4 probe (Phisitemp, Clifton, New Jersey). Seizures were identified by EEG recording and video analysis. First, mice were recorded at baseline for 15 min, and then seizures were evoked by progressively increasing the body temperature by 0.5°C every 30 s. The heating bulb was then promptly switched off to allow recovery; the mice were then monitored until the EEG and temperature returned to the baseline or until death occurred.

For EEG analysis, Neuroscore (Data Sciences International, St. Paul, MN) was used. For spike detection, EEG traces were first bandpass-filtered between 5 and 70 Hz. Threshold temperature, seizure duration, number of spikes during the attack, and spike frequency were considered. Spikes were detected by threshold analysis and then visually inspected to reject artifacts. All recordings and analysis were carried out blinded to the transduced viruses. Seizure severity was scored using a modification of the Racine scale.[66]

KA-Induced Febrile Seizures in Pups

A rectal temperature probe was used in P14–P17 pups to measure the basal body temperature before each injection. A single LPS injection (2 μg/mouse, Sigma, L4516) was administrated intraperitoneally (i.p.) 2 h before the experiment to induce fever and increase the temperature of the pups. Low-dose i.p. KA injections (5 mg/kg, Tocris, 0222) were performed every hour, and seizures were scored using the Racine scale every 10 min. Mice were culled after grade 5 was reached, and the time taken to reach grade 5 was used as a readout of seizure susceptibility. Seizure scoring was performed blinded to the identity of the injected virus.

Statistical Analysis

The results were analyzed with GraphPad Prism. Mean comparisons among different groups were performed with Student's t test or two-way ANOVA followed by Bonferroni's multiple comparisons test. In the case of non-normally distributed data, median comparisons between two groups were performed with a Mann-Whitney *U* test. The normality in the data distribution was assessed using the D'Agostino and Pearson omnibus test. For seizure score comparison, the chi-square test was employed. Individual statistical analyses and details regarding experimental design are described in detail alongside each experiment in Results and in the figure legends.

SUPPLEMENTAL INFORMATION

Supplemental Information can be found online at https://doi.org/10.1016/j.ymthe.2019.08.018.

AUTHOR CONTRIBUTIONS

G.C. and G.L. performed the experiments and analyzed data. C.D.B. designed and tested the sgRNAs and *Scn1a* transcriptional activation. J.C. performed *in vivo* WT experiments. N.V., G.M., and S. Bido performed viral injections in mice. L.M. developed the computational analysis. S. Brusco, V.C., S.M., and L.L. performed and analyzed the *in vivo* EEG recordings. S.G. produced AAVs. T.C. contributed to *in vitro* electrophysiology. F.B. contributed to analysis of the electrophysiological recordings. S.S. and D.M.K. contributed to the design of the experiments. V.B. supervised, coordinated, and supported the project and wrote the paper with G.C. and G.L.

CONFLICTS OF INTEREST

The authors declare no competing interests.

ACKNOWLEDGMENTS

We are thankful to Dr. K. Yamakawa for *Scn1a* mutant mice; L. Muzio, S. Levi, and D. Zacchetti for providing valuable reagents; S. Comai and M. Simonato for sharing the *in vivo* EEG recording instrumentation; C. Butti and E. Fraviga for technical help; and D. Bonanomi and all members of the Broccoli lab for helpful discussions. We acknowledge the FRACTAL core facility for expert supervision of flow cytometry. This work was supported by the Associazione Gruppo Famiglie Dravet (to V.B.), European Union FP7 Integrating Project "Desire" (602531 to F.B. and V.B.), the Cariplo Foundation (2016-0532 to G.C.), the Italian Ministry of Health (GR-2016-02363972 to G.C.), the Telethon Foundation (GGP19249 to G.C.), a Marie Curie individual fellowship (Marie Skłodowska-Curie grant agreement no. 658418 to G.L.), and an MRC gene therapy grant (MR/L01095X/1 to D.M.K. and S.S.).

REFERENCES

1. Kullmann, D.M. (2010). Neurological channelopathies. Annu. Rev. Neurosci. *33*, 151–172.
2. Dravet, C. (2011). Dravet syndrome history. Dev. Med. Child Neurol. *53*, 1–6.
3. Meisler, M.H., and Kearney, J.A. (2005). Sodium channel mutations in epilepsy and other neurological disorders. J. Clin. Invest. *115*, 2010-7.
4. Nickels, K.C., and Wirrell, E.C. (2017). Cognitive and Social Outcomes of Epileptic Encephalopathies. Semin. Pediatr. Neurol. *24*, 264–275.
5. Kasperaviciute, D., Catarino, C.B., Matarin, M., Leu, C., Novy, J., Tostevin, A., Leal, B., Hessel, E.V., Hallmann, K., Hildebrand, M.S., et al.; UK Brain Expression Consortium (2013). Epilepsy, hippocampal sclerosis and febrile seizures linked by common genetic variation around SCN1A. Brain *136*, 3140–3150.
6. Cetica, V., Chiari, S., Mei, D., Parrini, E., Grisotto, L., Marini, C., Pucatti, D., Ferrari, A., Sicca, F., Specchio, N., et al. (2017). Clinical and genetic factors predicting Dravet syndrome in infants with *SCN1A* mutations. Neurology *88*, 1037–1044.
7. Marini, C., Scheffer, I.E., Nabbout, R., Suls, A., De Jonghe, P., Zara, F., and Guerrini, R. (2011). The genetics of Dravet syndrome. Epilepsia *52* (*Suppl 2*), 24–29.
8. Yu, F.H., Mantegazza, M., Westenbroek, R.E., Robbins, C.A., Kalume, F., Burton, K.A., Spain, W.J., McKnight, G.S., Scheuer, T., and Catterall, W.A. (2006). Reduced sodium current in GABAergic interneurons in a mouse model of severe myoclonic epilepsy in infancy. Nat. Neurosci. *9*, 1142–1149.
9. Han, S., Tai, C., Westenbroek, R.E., Yu, F.H., Cheah, C.S., Potter, G.B., Rubenstein, J.L., Scheuer, T., de la Iglesia, H.O., and Catterall, W.A. (2012). Autistic-like behaviour in Scn1a+/- mice and rescue by enhanced GABA-mediated neurotransmission. Nature *489*, 385–390.

10. Ogiwara, I., Miyamoto, H., Morita, N., Atapour, N., Mazaki, E., Inoue, I., Takeuchi, T., Itohara, S., Yanagawa, Y., Obata, K., et al. (2007). Nav1.1 localizes to axons of parvalbumin-positive inhibitory interneurons: a circuit basis for epileptic seizures in mice carrying an Scn1a gene mutation. J. Neurosci. *27*, 5903–5914.

11. Ito, S., Ogiwara, I., Yamada, K., Miyamoto, H., Hensch, T.K., Osawa, M., and Yamakawa, K. (2013). Mouse with Nav1.1 haploinsufficiency, a model for Dravet syndrome, exhibits lowered sociability and learning impairment. Neurobiol. Dis. *49*, 29–40.

12. Hedrich, U.B.S., Liautard, C., Kirschenbaum, D., Pofahl, M., Lavigne, J., Liu, Y., Theiss, S., Slotta, J., Escayg, A., Dihné, M., et al. (2014). Impaired action potential initiation in GABAergic interneurons causes hyperexcitable networks in an epileptic mouse model carrying a human Na(V)1.1 mutation. J. Neurosci. *34*, 14874–14889.

13. Ogiwara, I., Iwasato, T., Miyamoto, H., Iwata, R., Yamagata, T., Mazaki, E., Yanagawa, Y., Tamamaki, N., Hensch, T.K., Itohara, S., and Yamakawa, K. (2013). Nav1.1 haploinsufficiency in excitatory neurons ameliorates seizure-associated sudden death in a mouse model of Dravet syndrome. Hum. Mol. Genet. *22*, 4784–4804.

14. Tai, C., Abe, Y., Westenbroek, R.E., Scheuer, T., and Catterall, W.A. (2014). Impaired excitability of somatostatin- and parvalbumin-expressing cortical interneurons in a mouse model of Dravet syndrome. Proc. Natl. Acad. Sci. USA *111*, E3139–E3148.

15. Tatsukawa, T., Ogiwara, I., Mazaki, E., Shimohata, A., and Yamakawa, K. (2018). Impairments in social novelty recognition and spatial memory in mice with conditional deletion of Scn1a in parvalbumin-expressing cells. Neurobiol. Dis. *112*, 24–34.

16. Oakley, J.C., Kalume, F., Yu, F.H., Scheuer, T., and Catterall, W.A. (2009). Temperature- and age-dependent seizures in a mouse model of severe myoclonic epilepsy in infancy. Proc. Natl. Acad. Sci. USA *106*, 3994–3999.

17. Wirrell, E.C. (2016). Treatment of Dravet Syndrome. Can. J. Neurol. Sci. *43*, S13–S18.

18. Chiron, C., and Dulac, O. (2011). The pharmacologic treatment of Dravet syndrome. Epilepsia *52* (*Suppl 2*), 72–75.

19. Griffin, A., Hamling, K.R., Knupp, K., Hong, S., Lee, L.P., and Baraban, S.C. (2017). Clemizole and modulators of serotonin signalling suppress seizures in Dravet syndrome. Brain *140*, 669–683.

20. Sourbron, J., Schneider, H., Kecskés, A., Liu, Y., Buening, E.M., Lagae, L., Smolders, I., and de Witte, P. (2016). Serotonergic Modulation as Effective Treatment for Dravet Syndrome in a Zebrafish Mutant Model. ACS Chem. Neurosci. *7*, 588–598.

21. Devinsky, O., Cross, J.H., and Wright, S. (2017). Trial of Cannabidiol for Drug-Resistant Seizures in the Dravet Syndrome. N. Engl. J. Med. *377*, 699–700.

22. Murlidharan, G., Samulski, R.J., and Asokan, A. (2014). Biology of adeno-associated viral vectors in the central nervous system. Front. Mol. Neurosci. *7*, 76.

23. Kay, M.A., Glorioso, J.C., and Naldini, L. (2001). Viral vectors for gene therapy: the art of turning infectious agents into vehicles of therapeutics. Nat. Med. *7*, 33–40.

24. Wright, A.V., Nuñez, J.K., and Doudna, J.A. (2016). Biology and Applications of CRISPR Systems: Harnessing Nature's Toolbox for Genome Engineering. Cell *164*, 29–44.

25. Hsu, P.D., Lander, E.S., and Zhang, F. (2014). Development and applications of CRISPR-Cas9 for genome engineering. Cell *157*, 1262–1278.

26. Mali, P., Aach, J., Stranges, P.B., Esvelt, K.M., Moosburner, M., Kosuri, S., Yang, L., and Church, G.M. (2013). CAS9 transcriptional activators for target specificity screening and paired nickases for cooperative genome engineering. Nat. Biotechnol. *31*, 833–838.

27. Dominguez, A.A., Lim, W.A., and Qi, L.S. (2016). Beyond editing: repurposing CRISPR-Cas9 for precision genome regulation and interrogation. Nat. Rev. Mol. Cell Biol. *17*, 5–15.

28. Sander, J.D., and Joung, J.K. (2014). CRISPR-Cas systems for editing, regulating and targeting genomes. Nat. Biotechnol. *32*, 347–355.

29. Liu, J., Gao, C., Chen, W., Ma, W., Li, X., Shi, Y., Zhang, H., Zhang, L., Long, Y., Xu, H., et al. (2016). CRISPR/Cas9 facilitates investigation of neural circuit disease using human iPSCs: mechanism of epilepsy caused by an SCN1A loss-of-function mutation. Transl Psychiatry *6*, e703.

30. Liao, H.-K., Hatanaka, F., Araoka, T., Reddy, P., Wu, M.Z., Sui, Y., Yamauchi, T., Sakurai, M., O'Keefe, D.D., Núñez-Delicado, E., et al. (2017). In Vivo Target Gene Activation via CRISPR/Cas9-Mediated Trans-epigenetic Modulation. Cell *171*, 1495–1507.e15.

31. Hilton, I.B., D'Ippolito, A.M., Vockley, C.M., Thakore, P.I., Crawford, G.E., Reddy, T.E., and Gersbach, C.A. (2015). Epigenome editing by a CRISPR-Cas9-based acetyltransferase activates genes from promoters and enhancers. Nat. Biotechnol. *33*, 510–517.

32. Liu, X.S., Wu, H., Ji, X., Stelzer, Y., Wu, X., Czauderna, S., Shu, J., Dadon, D., Young, R.A., and Jaenisch, R. (2016). Editing DNA Methylation in the Mammalian Genome. Cell *167*, 233–247.e17.

33. Zhou, H., Liu, J., Zhou, C., Gao, N., Rao, Z., Li, H., Hu, X., Li, C., Yao, X., Shen, X., et al. (2018). In vivo simultaneous transcriptional activation of multiple genes in the brain using CRISPR-dCas9-activator transgenic mice. Nat. Neurosci. *21*, 440–446.

34. Konermann, S., Brigham, M.D., Trevino, A.E., Joung, J., Abudayyeh, O.O., Barcena, C., Hsu, P.D., Habib, N., Gootenberg, J.S., Nishimasu, H., et al. (2015). Genome-scale transcriptional activation by an engineered CRISPR-Cas9 complex. Nature *517*, 583–588.

35. Simeonov, D.R., Gowen, B.G., Boontanrart, M., Roth, T.L., Gagnon, J.D., Mumbach, M.R., Satpathy, A.T., Lee, Y., Bray, N.L., Chan, A.Y., et al. (2017). Discovery of stimulation-responsive immune enhancers with CRISPR activation. Nature *549*, 111–115.

36. Gilbert, L.A., Larson, M.H., Morsut, L., Liu, Z., Brar, G.A., Torres, S.E., Stern-Ginossar, N., Brandman, O., Whitehead, E.H., Doudna, J.A., et al. (2013). CRISPR-mediated modular RNA-guided regulation of transcription in eukaryotes. Cell *154*, 442–451.

37. Kearns, N.A., Genga, R.M., Enuameh, M.S., Garber, M., Wolfe, S.A., and Maehr, R. (2014). Cas9 effector-mediated regulation of transcription and differentiation in human pluripotent stem cells. Development *141*, 219–223.

38. Matharu, N., Rattanasopha, S., Tamura, S., Maliskova, L., Wang, Y., Bernard, A., Hardin, A., Eckalbar, W.L., Vaisse, C., and Ahituv, N. (2019). CRISPR-mediated activation of a promoter or enhancer rescues obesity caused by haploinsufficiency. Science *363*, eaau0629.

39. Nakayama, T., Ogiwara, I., Ito, K., Kaneda, M., Mazaki, E., Osaka, H., Ohtani, H., Inoue, Y., Fujiwara, T., Uematsu, M., et al. (2010). Deletions of SCN1A 5′ genomic region with promoter activity in Dravet syndrome. Hum. Mutat. *31*, 820–829.

40. Grubb, M.S., and Burrone, J. (2010). Activity-dependent relocation of the axon initial segment fine-tunes neuronal excitability. Nature *465*, 1070–1074.

41. Morris, G., Leite, M., Kullmann, D.M., Pavlov, I., Schorge, S., and Lignani, G. (2017). Activity Clamp Provides Insights into Paradoxical Effects of the Anti-Seizure Drug Carbamazepine. J. Neurosci. *37*, 5484–5495.

42. Cheah, C.S., Westenbroek, R.E., Roden, W.H., Kalume, F., Oakley, J.C., Jansen, L.A., and Catterall, W.A. (2013). Correlations in timing of sodium channel expression, epilepsy, and sudden death in Dravet syndrome. Channels (Austin) *7*, 468–472.

43. Hammond, S.L., Leek, A.N., Richman, E.H., and Tjalkens, R.B. (2017). Cellular selectivity of AAV serotypes for gene delivery in neurons and astrocytes by neonatal intracerebroventricular injection. PLoS ONE *12*, e0188830.

44. Dimidschstein, J., Chen, Q., Tremblay, R., Rogers, S.L., Saldi, G.A., Guo, L., Xu, Q., Liu, R., Lu, C., Chu, J., et al. (2016). A viral strategy for targeting and manipulating interneurons across vertebrate species. Nat. Neurosci. *19*, 1743–1749.

45. Stühmer, T., Puelles, L., Ekker, M., and Rubenstein, J.L.R. (2002). Expression from a Dlx gene enhancer marks adult mouse cortical GABAergic neurons. Cereb. Cortex *12*, 75–85.

46. Eun, B.-L., Abraham, J., Mlsna, L., Kim, M.J., and Koh, S. (2015). Lipopolysaccharide potentiates hyperthermia-induced seizures. Brain Behav. *5*, e00348.

47. Heida, J.G., Teskey, G.C., and Pittman, Q.J. (2005). Febrile convulsions induced by the combination of lipopolysaccharide and low-dose kainic acid enhance seizure susceptibility, not epileptogenesis, in rats. Epilepsia *46*, 1898–1905.

48. Schmidt, J.W., and Catterall, W.A. (1986). Biosynthesis and processing of the α subunit of the voltage-sensitive sodium channel in rat brain neurons. Cell *46*, 437–444.

49. Chavez, A., Tuttle, M., Pruitt, B.W., Ewen-Campen, B., Chari, R., Ter-Ovanesyan, D., Haque, S.J., Cecchi, R.J., Kowal, E.J.K., Buchthal, J., et al. (2016). Comparison of Cas9 activators in multiple species. Nat. Methods *13*, 563–567.

50. Staahl, B.T., Benekareddy, M., Coulon-Bainier, C., Banfal, A.A., Floor, S.N., Sabo, J.K., Urnes, C., Munares, G.A., Ghosh, A., and Doudna, J.A. (2017). Efficient genome editing in the mouse brain by local delivery of engineered Cas9 ribonucleoprotein complexes. Nat. Biotechnol. *35*, 431–434.

51. Swiech, L., Heidenreich, M., Banerjee, A., Habib, N., Li, Y., Trombetta, J., Sur, M., and Zhang, F. (2015). In vivo interrogation of gene function in the mammalian brain using CRISPR-Cas9. Nat. Biotechnol. *33*, 102–106.

52. Rhodes, T.H., Lossin, C., Vanoye, C.G., Wang, D.W., and George, A.L., Jr. (2004). Noninactivating voltage-gated sodium channels in severe myoclonic epilepsy of infancy. Proc. Natl. Acad. Sci. USA *101*, 11147–11152.

53. Catarino, C.B., Liu, J.Y., Liagkouras, I., Gibbons, V.S., Labrum, R.W., Ellis, R., Woodward, C., Davis, M.B., Smith, S.J., Cross, J.H., et al. (2011). Dravet syndrome as epileptic encephalopathy: evidence from long-term course and neuropathology. Brain *134*, 2982–3010.

54. Mendell, J.R., Al-Zaidy, S., Shell, R., Arnold, W.D., Rodino-Klapac, L.R., Prior, T.W., Lowes, L., Alfano, L., Berry, K., Church, K., et al. (2017). Single-Dose Gene-Replacement Therapy for Spinal Muscular Atrophy. N. Engl. J. Med. *377*, 1713–1722.

55. Chen, B., Hu, J., Almeida, R., Liu, H., Balakrishnan, S., Covill-Cooke, C., Lim, W.A., and Huang, B. (2016). Expanding the CRISPR imaging toolset with *Staphylococcus aureus* Cas9 for simultaneous imaging of multiple genomic loci. Nucleic Acids Res. *44*, e75.

56. Harrington, L.B., Paez-Espino, D., Staahl, B.T., Chen, J.S., Ma, E., Kyrpides, N.C., and Doudna, J.A. (2017). A thermostable Cas9 with increased lifetime in human plasma. Nat. Commun. *8*, 1424.

57. Kim, E., Koo, T., Park, S.W., Kim, D., Kim, K., Cho, H.Y., Song, D.W., Lee, K.J., Jung, M.H., Kim, S., et al. (2017). In vivo genome editing with a small Cas9 orthologue derived from Campylobacter jejuni. Nat. Commun. *8*, 14500.

58. Davis, C.A., Hitz, B.C., Sloan, C.A., Chan, E.T., Davidson, J.M., Gabdank, I., Hilton, J.A., Jain, K., Baymuradov, U.K., Narayanan, A.K., et al. (2018). The Encyclopedia of DNA elements (ENCODE): data portal update. Nucleic Acids Res. *46* (D1), D794–D801.

59. Carninci, P., Sandelin, A., Lenhard, B., Katayama, S., Shimokawa, K., Ponjavic, J., Semple, C.A., Taylor, M.S., Engström, P.G., Frith, M.C., et al. (2006). Genome-wide analysis of mammalian promoter architecture and evolution. Nat. Genet. *38*, 626–635.

60. Thorvaldsdóttir, H., Robinson, J.T., and Mesirov, J.P. (2013). Integrative Genomics Viewer (IGV): high-performance genomics data visualization and exploration. Brief. Bioinform. *14*, 178–192.

61. Cheng, A.W., Wang, H., Yang, H., Shi, L., Katz, Y., Theunissen, T.W., Rangarajan, S., Shivalila, C.S., Dadon, D.B., and Jaenisch, R. (2013). Multiplexed activation of endogenous genes by CRISPR-on, an RNA-guided transcriptional activator system. Cell Res. *23*, 1163–1171.

62. Colasante, G., Lignani, G., Rubio, A., Medrihan, L., Yekhlef, L., Sessa, A., Massimino, L., Giannelli, S.G., Sacchetti, S., Caiazzo, M., et al. (2015). Rapid Conversion of Fibroblasts into Functional Forebrain GABAergic Interneurons by Direct Genetic Reprogramming. Cell Stem Cell *17*, 719–734.

63. Tamamaki, N., Yanagawa, Y., Tomioka, R., Miyazaki, J., Obata, K., and Kaneko, T. (2003). Green fluorescent protein expression and colocalization with calretinin, parvalbumin, and somatostatin in the GAD67-GFP knock-in mouse. J. Comp. Neurol. *467*, 60–79.

64. Langmead, B., Trapnell, C., Pop, M., and Salzberg, S.L. (2009). Ultrafast and memory-efficient alignment of short DNA sequences to the human genome. Genome Biol. *10*, R25.

65. Love, M.I., Huber, W., and Anders, S. (2014). Moderated estimation of fold change and dispersion for RNA-seq data with DESeq2. Genome Biol. *15*, 550.

66. Velíšková, J., and Velíšek, L. (2017). Behavioral characterization and scoring of seizures in rodents. In Models of Seizures and Epilepsy, A. Pitkänen, P.S. Buckmaster, A.S. Galanopoulou, and S.L. Moshé, eds. (Academic Press), pp. 111–123.

YMTHE, Volume *28*

Supplemental Information

dCas9-Based *Scn1a* Gene Activation Restores Inhibitory Interneuron Excitability and Attenuates Seizures in Dravet Syndrome Mice

Gaia Colasante, Gabriele Lignani, Simone Brusco, Claudia Di Berardino, Jenna Carpenter, Serena Giannelli, Nicholas Valassina, Simone Bido, Raffaele Ricci, Valerio Castoldi, Silvia Marenna, Timothy Church, Luca Massimino, Giuseppe Morabito, Fabio Benfenati, Stephanie Schorge, Letizia Leocani, Dimitri M. Kullmann, and Vania Broccoli

Figure S1. Related to Figure 1

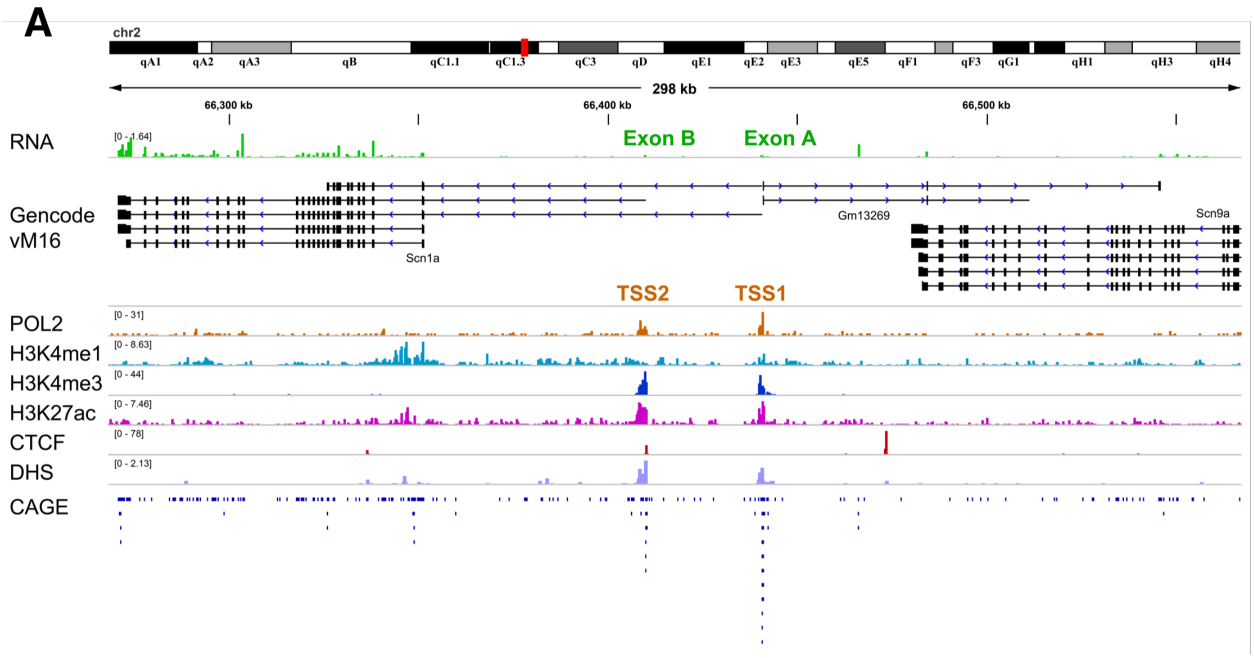

Figure S2. Related to Figure 1

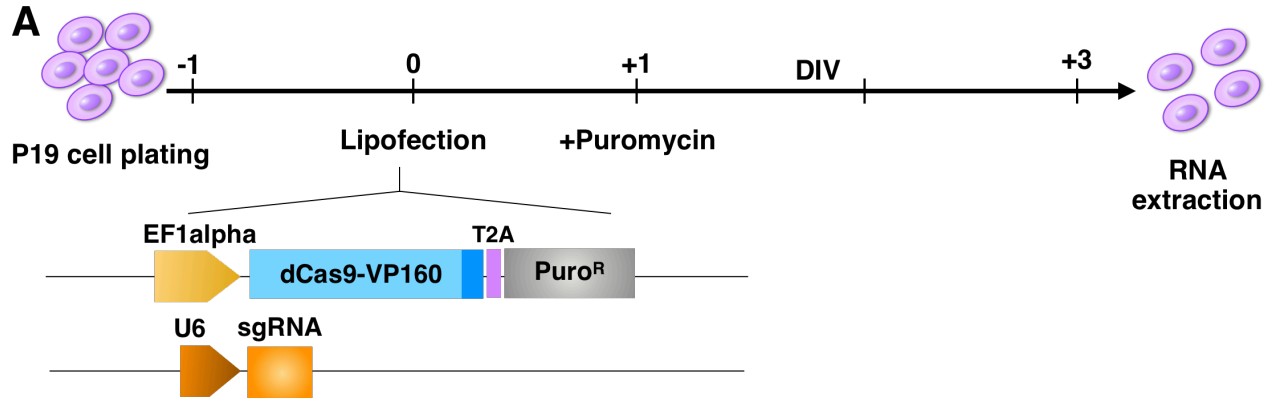

P19 cells

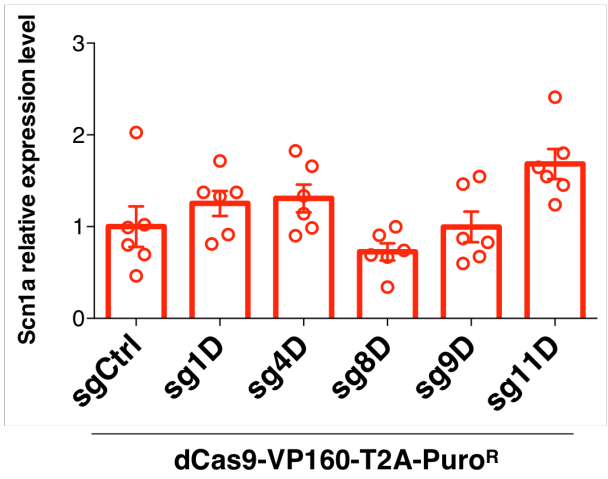

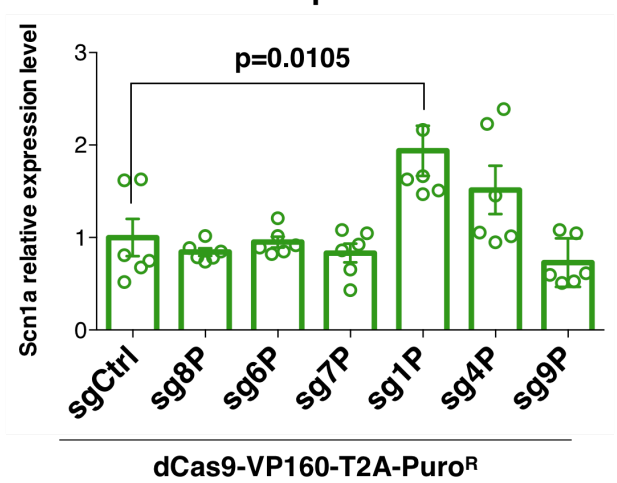

MEFs

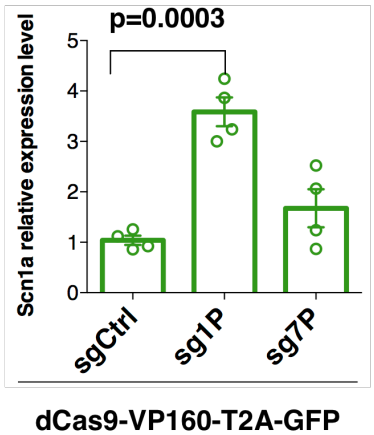

Figure S3. Related to Figure 4

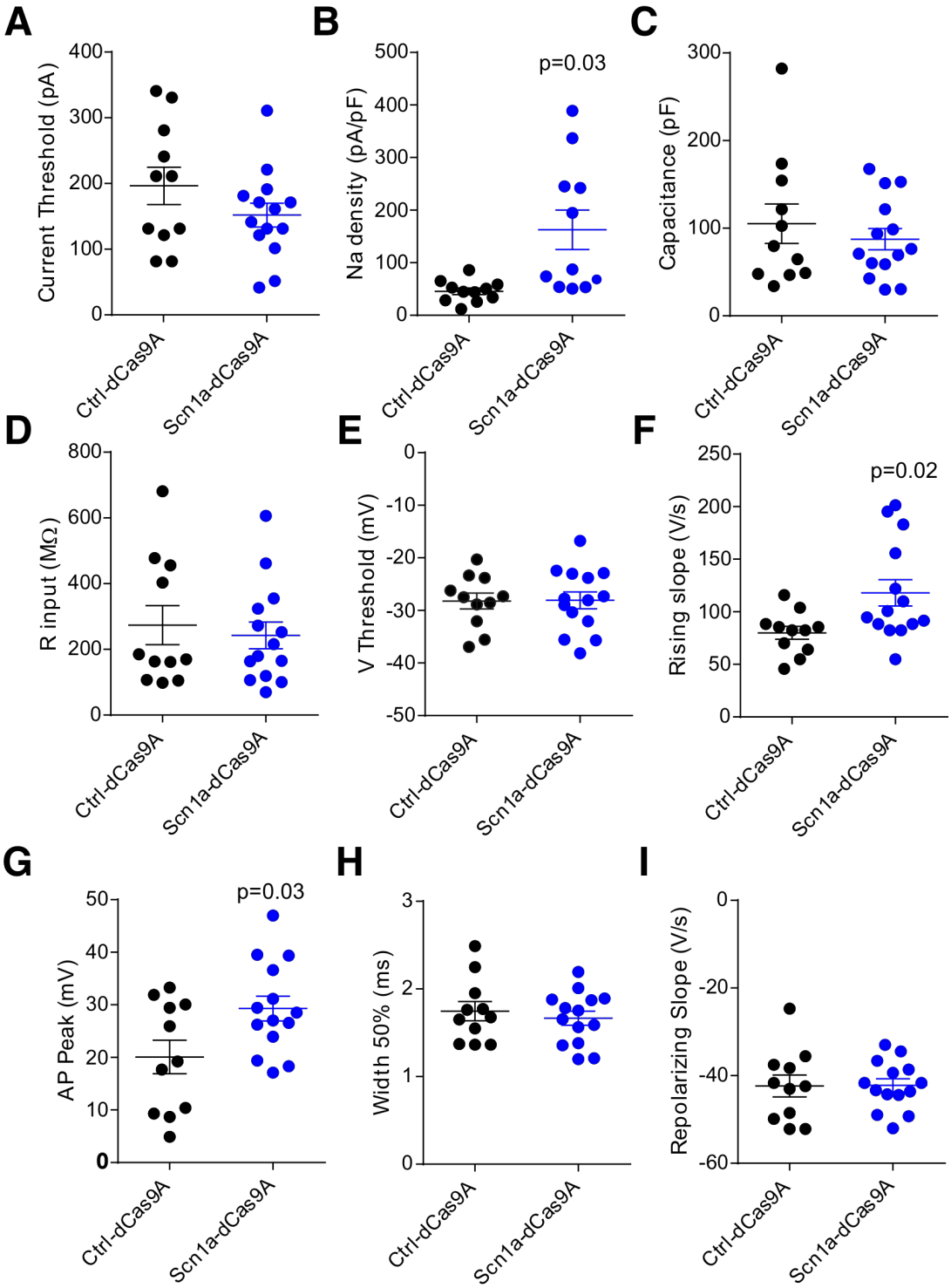

Figure S4. Related to Figure 4

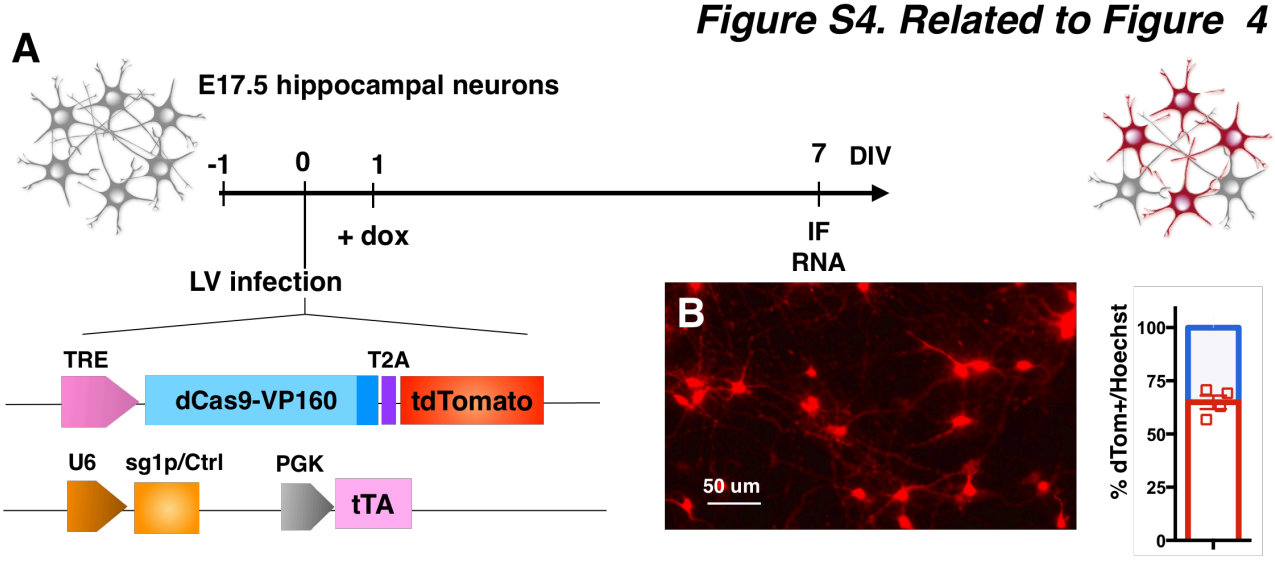

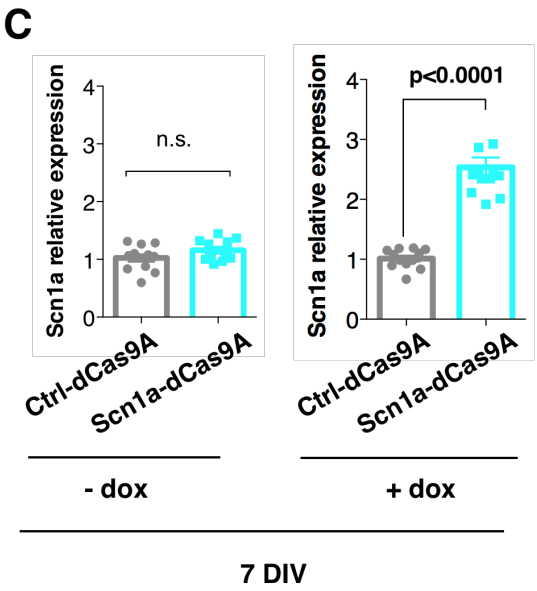

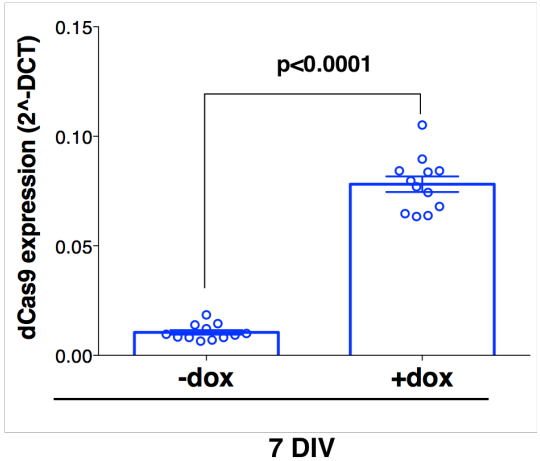

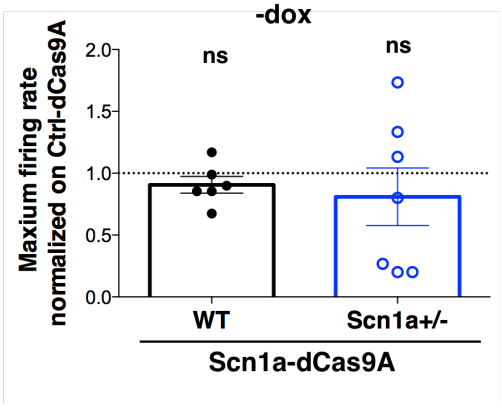

Figure S5. Related to Figure 6

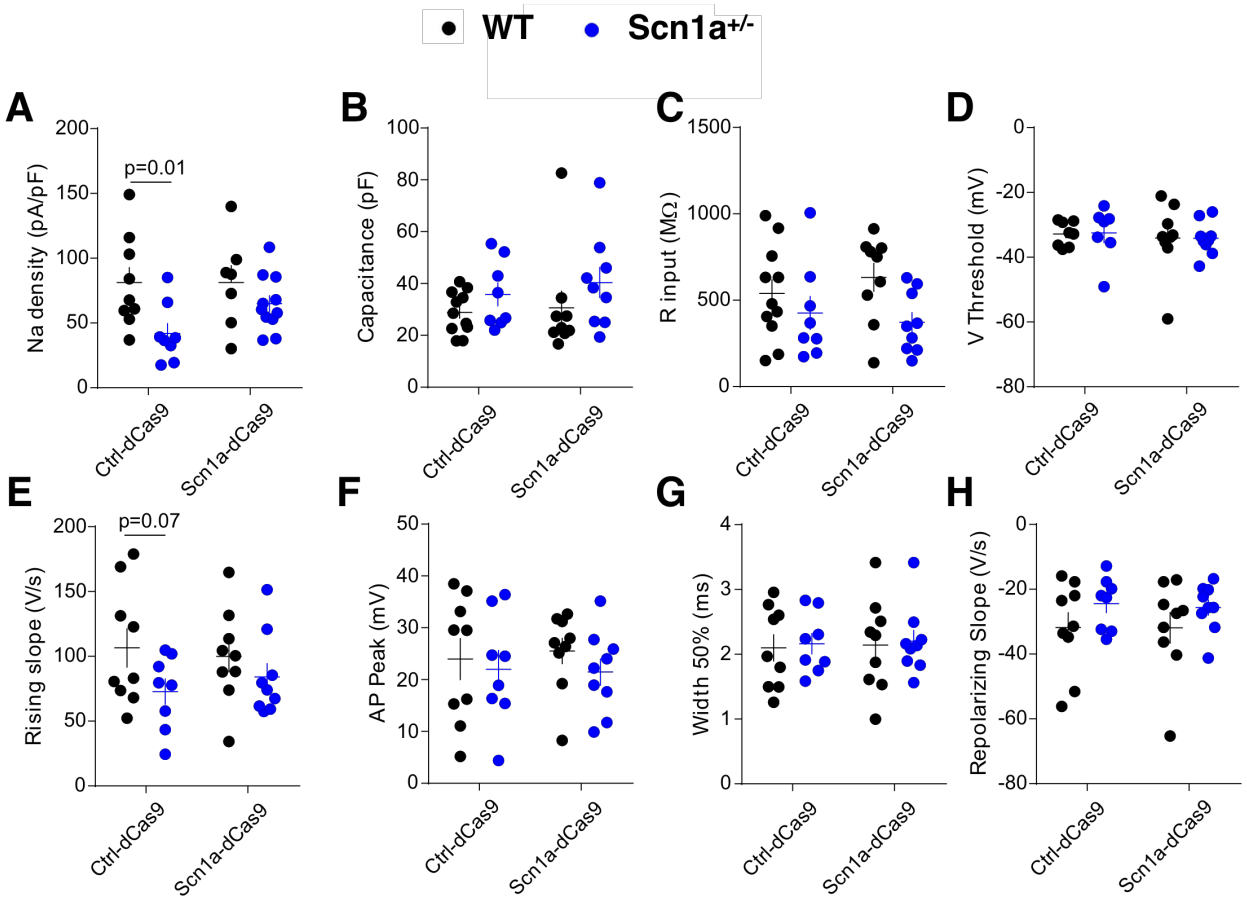

Figure S6. Related to Figure 7

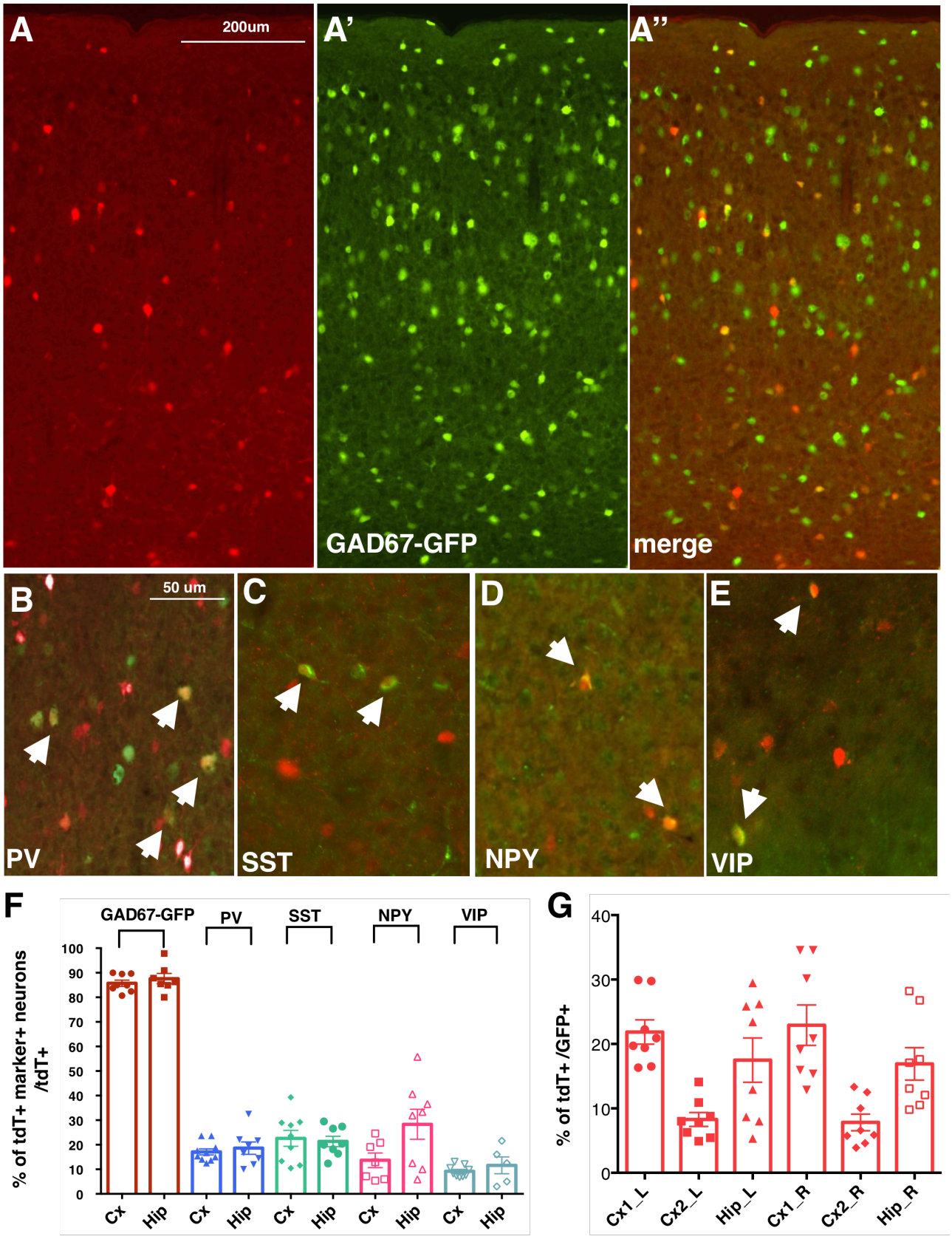

Figure S7. Related to Figure 7

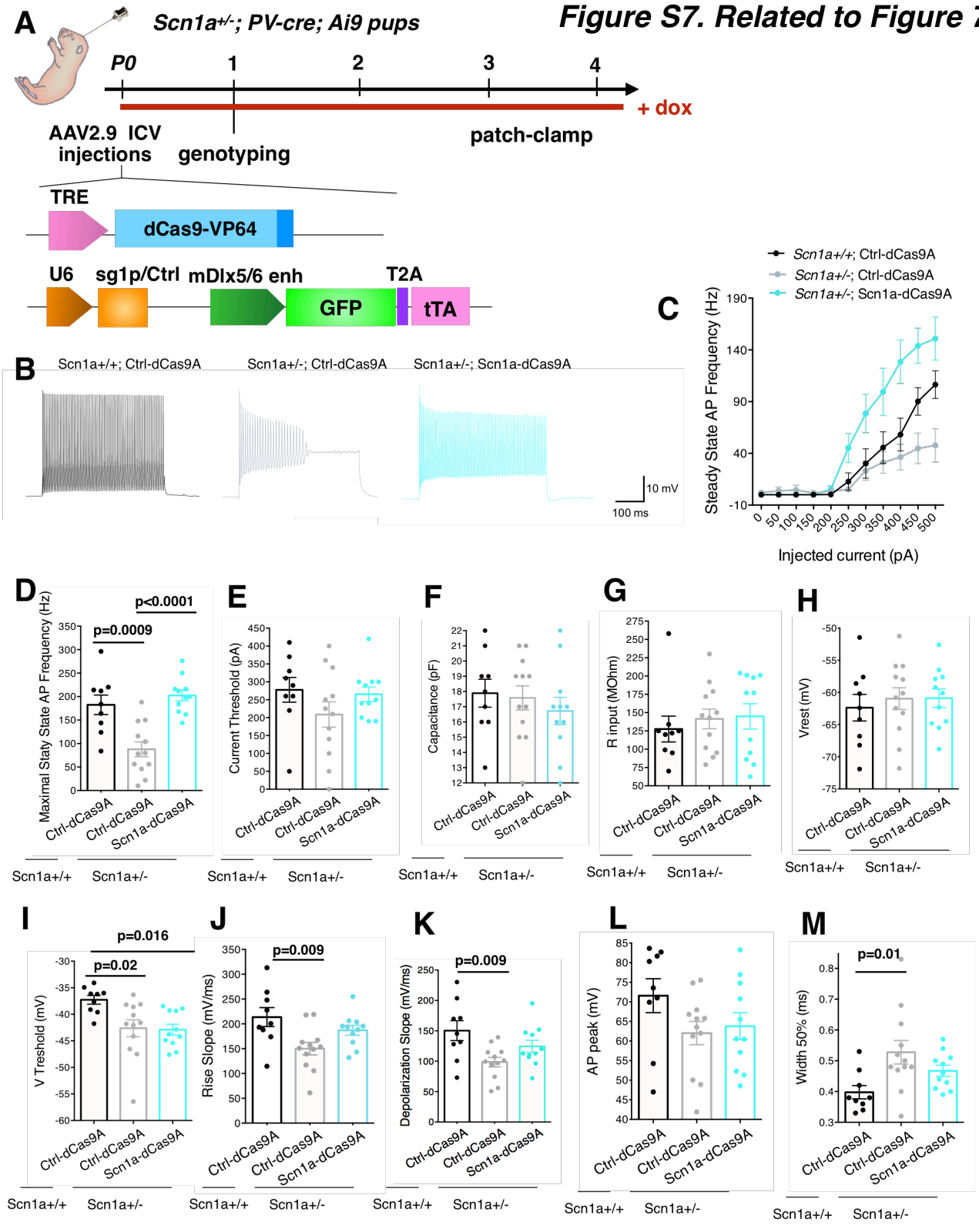

Figure S8. Related to Figure 7

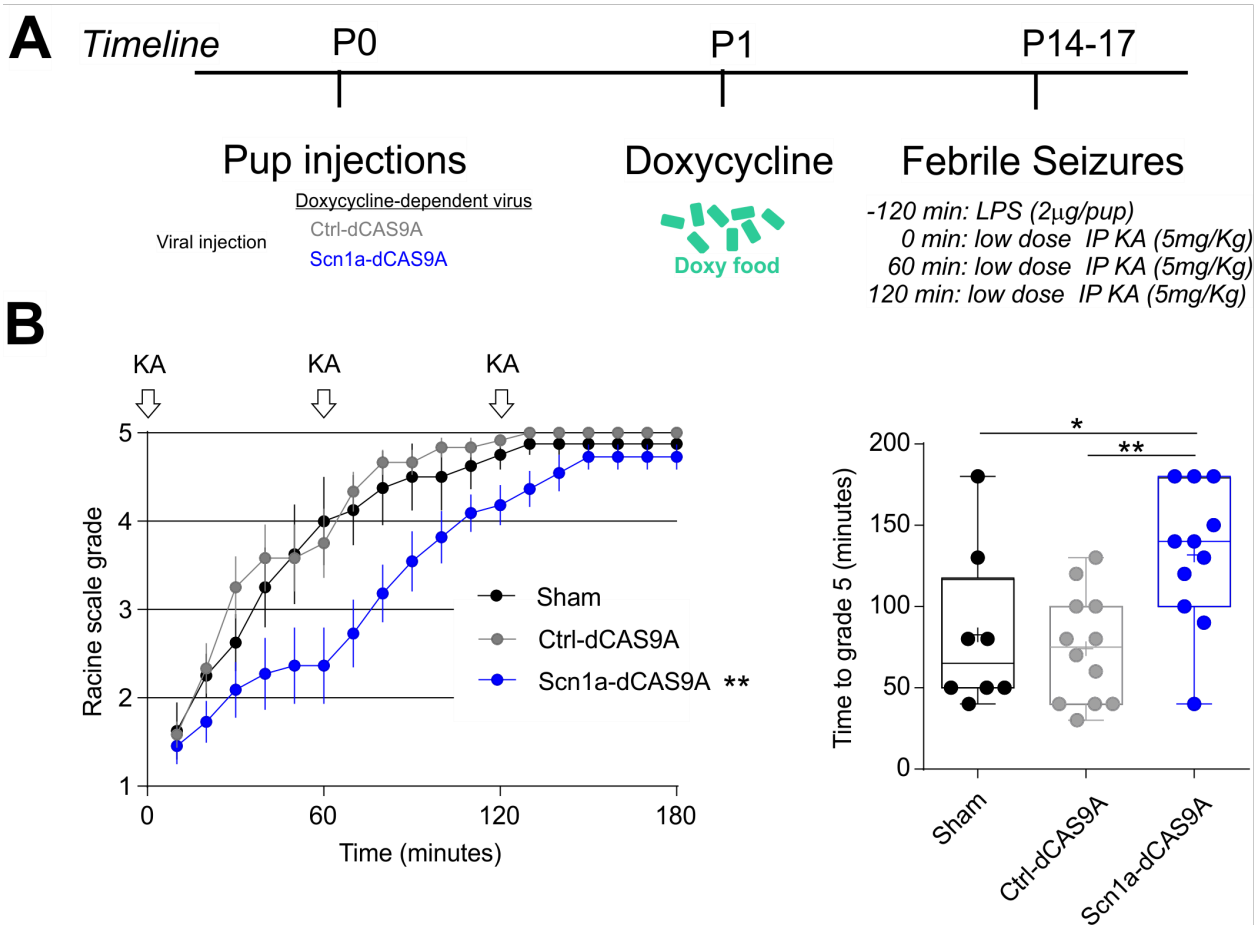

Table S1: Sequences of sgRNAs

sg1D	CGTTTTTGAAACGTTTTGGA AGG
sg4D	AGCATGAAAGCTAAATCTCC TGG
sg8D	ATAGGTCTCATTTTGTGGGT AGG
sg9D	TTGCATGGAAATCATGAACC AGG
sg11D	AAGTATTGGCAGCAGCAAGC AGG
sg8P	AATAAGCAAATTTCATTCAT GGG
sg6P	ATTGTTACTTTTACAGATTA CGG
sg7P	CCCCTTTGCTCTGCCTATCA TGG
sg1P	TAAGTCAATAGTTCCATGAT AGG
sg9P	CCCCTTTGCTCTGCCTATCA TGG
sg4P	CCATGATAGGCAGAGCAAAG TGG
sglacZ	TGCGAATACGCCCACGCGAT

Table S2: Primers for RT-qPCR

18s_F	GGTGAAATTCTTGGACCGGC
18s_R	GACTTTGGTTTCCCGGAAGC
Scn1a_F	CACCAACGCTTCCCTTGAGG
Scn1a_R	TGGACATTGGCCTGCATCAG
Scn1a_exA_F	GGTCCTGGTGGTACAAGCACT
Scn1a_exA_R	GAGGCTGCAGGAAGCTGAG
Scn2a_F	CCTCAGGAGGTCTATGCCAAA
Scn2a_R	GTGTCAGCTGGTTGCGAAAA
Scn3a_F	GCATTGCGTCCACGTAGATAA
Scn3a_R	GGAGCTGAAGACATGGGTCA
Scn4a_F	AGATCCCGCCTCCTGATTTA
Scn4a_R	ATCATGGGGGTGAGAGGAGT
Scn5a_F	TGGGAGAGGAGACAGTGTGG
Scn5a_R	CACGGGGATGATTGGACTTA
Scn7a_F	CCTTACCAACTTGCCTTGGA
Scn7a_R	ACCAACCAACCAACCAAACA
Scn8a_F	GCTTCTGCCATATCCCTCCA
Scn8a_R	GGCAGCTCCATCTTTCCATC
Scn9a_F	ATGGAAGATGCCAAGCAGTG
Scn9a_R	TGGATGTTTTGTGTGGCTCA
Scn10a_F	TCCCACCATCCTATGACAGC
Scn10a_R	ACTGAGGTCCAGGGCTCTTC
Scn11a_F	TTCATGGAGGCCAATCCTTT
Scn11a_R	TGACCTGCCTTTCAGCTTCA
Pde4b_F	TCAGCCAGGTCTAATCTGCCA
Prp4_F	GGTCCATGGTGACCTTCAAGA
Prp4_R	ATGTGGACTGTAGGTGGTGC
BC02_F	AGTGAGTGCAGGGGTCCT
BC02_R	GAAGGATGGTGGTTGGTGGG
Olfr919_F	CCTGGATGGTAGGTGGGGTA
Olfr919_R	GCAGGCAAGCTCCATCAATG
Plrg1_F	AGTTGCTACCGTGAGATGCC
Plrg1_R	TGGTTCGTCAGTGTCACTCG

Supplementary Figure Legends

Figure S1 | Bioinformatics analysis of the *Scn1a* gene locus for promoter regulatory region prediction.

Alignment to the *Scn1a* gene reference sequence of RNA-seq, ChIP-seqs, DNase-seq and CAGE- seq profiles related to adult mouse brains. The enrichment of markers associated with transcriptional activation in the regions upstream of the first two untranslated exons (Exon A and Exon B) of the gene highlights the presence of two TSS (TSS1 and TSS2) and allows to localize a distal promoter in the 200 bp upstream of exon-A and a proximal promoter upstream of the exon-B. POL2, RNA polymerase II ChIP-seq; H3K4me3, tri-methylation of lysine 4 on the histone H3 ChIP-seq; H3K4me1, mono- methylation of lysine 4 on histone H3 ChIP-seq; H3K27ac, acetylation of lysine 27 on histone H3 ChIP-seq; CTCF, factor that binds the CCCTC; DHS, DNase I Hyper Sensitivity mapping; CAGE-seq, Cap Analysis of Gene Expression-sequencing.

Figure S2 | Screening of sgRNAs for *Scn1a* gene activation by targeting its distal or proximal promoter in association with the dCas9-VP160-T2A-GFP in different cell types.

a, Screening of the guides lipofected in P19 cells in association with dCas9VP160-T2A-Puro^R. Quantitative RT-PCRs performed on RNA extracted from P19 cells 3 days after lipofection with dCas9VP160-T2A-Puro^R and sgRNAs targeting distal **(b)** or proximal **(c)** promoters to evaluate levels of *Scn1a* gene transcript. Data are normalized on 18S rRNA and relative to sgCtrl lipofected cells; n = 6, p = 0.0001, one-way ANOVA followed by Bonferroni multi comparison tests. **d**, RT-qPCR on RNA extracted from MEFs infected with sg1P and sg7P in association with dCas9VP160-T2A-Puro^R; n = 4, p = 0.0003, One-way ANOVA followed by Bonferroni's multiple comparison tests. Data are shown as mean ± s.e.m. with dots representing individual samples.

Figure S3 | The *Scn1a*-dCas9A system accelerates functional maturation of primary wild-type hippocampal neurons at 9-11 DIV.

Analysis of passive properties, voltage steps and current threshold (**a-d**), and single AP shape (**e-i**) in 9-11 DIV wild-type primary neurons transduced with either the Ctrl-dCas9A or *Scn1a*-dCas9A system. Student's *t* test was used for statistical analysis.

Figure S4 | Assessing the leakiness of the *Scn1a* gene activation by the *Scn1a*-dCas9A system.

A, Illustration of the dual LV doxycycline (dox) inducible system set for patch-clamp experiments *in vitro:* a first LV carrying dCas9-VP160 regulated by the rtTA responsive element (TRE) and a second

carrying the transactivator rtTA together with the sgRNA. Dox was administered or not at / DIV IF and RNA extraction were performed; **B**, anti-RFP immunofluorescence and quantification of tdTomato^{+} transduced cells over total neurons. **C**, Relative RT-qPCR for Scn1a performed on RNA extracted from either Ctrl-dCas9A or *Scn1a*-dCasA in WT neurons at 7 DIV in the absence or presence of dox. Data are expressed as ratios relative to Ctrl-dCas9A. **D,** RT-qPCR for dCas9 (2^-DCt) in neurons transduced with Scn1a-dCas9A system in the absence or presence of dox (n=12, $p<0.0001$ Student's *t* test. **E,** Histogram plot of maximum firing rate in Scn1a-dCas9A treated wt and Scn1a$^{+/-}$ GAD67-GFP neurons relative to Ctrl-dCas9A in the absence of dox (n=7, Student's *t* test).

Figure S5| The *Scn1a*-dCas9 system corrects some functional impairments in 18-20 DIV primary *Scn1a*$^{+/-}$ neurons while is not altering activity in corresponding wild-type neurons.
A-H, Analysis of passive properties, Na^{+} current density and single AP shape in *Scn1a*$^{+/+}$ (black dots) and *Scn1a*$^{+/-}$ (blue dots) primary neurons transduced with either the Ctrl-dCas9A or the *Scn1a*-dCas9A system.

Figure S6 | AAVs packaged with the Scn1a-dCas9A system controlled by the Dlx5/6 enhancer direct tdTomato expression specifically in cortical interneuron subpopulations *in vivo*.
A-A'', Anti-GFP and anti-RFP dual immunofluorescence in brain sections of P30 GAD67-GFP mice subjected to intracerebroventricular injections at P0 with AAVs carrying *Scn1a*-dCas9A elements, scale bars 200um. **B-E**, Representative cortical areas of P30 mouse brain sections transduced at P0 with the *Scn1a*- dCas9A elements stained for anti-PV, -SST, -NPY and -VIP in association with anti-RFP to reveal transduced neurons, scale bars 50 um. **F,** Quantification of the percentage of tdTomato^{+} cells co-expressing each of the interneuron markers listed above (GAD67-GFP, PV, SST, NPY and VIP) over the total number of tdTomato^{+} cells. **G**, Quantifications of the percentage of tdTomato^{+} cells over the total of GAD67-GFP+ cells in various areas (Cx1, Cx2 and Hip in each brain hemisphere). Data are shown as mean ± s.e.m., with dots representing individual quantifications.

Figure S7 | Scn1a-dCas9A treatment ameliorates firing in Scn1a+/- PV interneurons
A, Schematic illustration showing the experimental setting for ICV injections of Ctrl and Scn1a-dCas9A with GFP reporter into *Scn1a*$^{+/+}$ and *Scn1a*$^{+/-}$; PV-Cre Ai9 P0 pups. Transduced PV interneurons appear GFP^{+} and tdTomato^{+}. Dox was administered in drinking water until the final analysis. **B**, Representative traces recorded from GFP^{+}/tdTomato PV^{+} interneurons in somatosensory cortex (SSC) (P21-28). **C**, I/O plot analysis show impaired functionality in *Scn1a*$^{+/-}$ Ctrl-dCas9A compared to *Scn1a*$^{+/+}$; Ctrl-dCas9A interneurons which is recovered in *Scn1a*$^{+/-}$;Scn1a-dCas9A PV

interneurons (p=0.003, two-way ANOVA/Bonferroni). **D.** Maximal steady state AP frequency and other passive and AP parameters of *Scn1a*$^{+/+}$; Ctrl-dCas9A and *Scn1a*$^{+/-}$; Ctrl-/ Scn1a-dCas9A transduced PV interneurons (one-way ANOVA/Bonferroni's multiple comparison tests).

Figure S8 | Upregulation of Nav1.1 during early development is protective against febrile seizures. A. Timeline of the experimental plan. **B.** *Left.* Racine scale scoring following low dose KA injections every hour over a 3-hour experimental time period with behavioural scoring every 10 minutes. ** $p<0.01$, two-way ANOVA, Sham or Ctrl-dCAS9A vs Scn1a-dCAS9A. *Right.* Box plots of the time taken to reach grade 5. Middle line represents the median, "+" the mean and the box, the 10-90 percentile range. *$p<0.05$, **$p<0.01$, one-way ANOVA followed by Bonferroni multi-comparison test.

Supplementary Table 1: Sequences of sgRNAs.

Supplementary Table 2: Primers for RT-qPCRs.